Aus der Klinik für Neurochirurgie

Geschäftsführender Direktor: Prof. Dr. Christopher Nimsky

des Fachbereichs Medizin der Philipps-Universität Marburg

Title der Dissertation:

Advanced Application of Diffusion Kurtosis Imaging

Inaugural-Dissertation zur Erlangung des Doktorgrades der gesamten Humanmedizin

dem Fachbereich Medizin der Philipps-Universität Marburg

vorgelegt von

Xinman Liu

aus Yangjiang, VR China

Marburg, 2020

Angenommen vom Fachbereich Medizin der Philipps-Universität Marburg

am: 15. September 2020

Gedruckt mit Genehmigung des Fachbereichs Medizin

Dekan: Prof. Dr. Helmut Schäfer

Referent: Prof. Dr. Christopher Nimsky

1. Korreferent: Prof. Dr. Andreas Jansen

This is dedicated to my beloved parents Kaiyun Liu and Xianjiao Zhang.

Table of Contents

Abbreviations

ADC	apparent diffusion coefficient
AF	arcuate fasciculus
ATR	anterior thalamic radiation
CB	cingulum bundle
CST	corticospinal tract
DKI	diffusion kurtosis imaging
DSI	diffusion spectrum imaging
DTI	diffusion tensor imaging
EOR	extent of resection
EPI	echo-planar imaging
FA	fractional anisotropy
FLAIR	fluid-attenuated inversion recovery
Fma	forceps major
Fmi	forceps minor
fMRI	functional magnetic resonance imaging
FoV	field of view
FSL	FMRIB Software Library
IFOF	inferior fronto-occipital fasciculus
ILF	inferior longitudinal fasciculus
JHU	Johns Hopkins University
KPS	Karnofsky Performance Status
LI	laterality index
MD	mean diffusivity
MEPs	motor-evoked potentials
MK	mean kurtosis
MNI	Montreal Neuroscience Institute
MRI	magnetic resonance imaging

NMR	nuclear magnetic resonance
ODF	orientation distribution function
PLIC	posterior limb of internal capsule
QBI	q-ball imaging
QSDR	q-space diffeomorphic reconstruction
ROI	regions of interest
SD	standard deviation
SLF	superior longitudinal fasciculus
TBSS	tract-based spatial statistics
TE	echo time
TR	repetition time
UF	uncinate fasciculus
VBM	voxel-based morphometry

List of Tables

List of Figures

1 Introduction

1.1 Diffusion-weighted imaging and diffusion tensor imaging

Diffusion tensor imaging (DTI) is commonly used in neurosurgery and neuroscience because of its capability to reconstruct white matter fiber tracts in the brain. Visualization of these reconstructed tracts can help guide neurosurgical procedures in order to preserve neurological functions. White matter fibers can be divided into three groups – projection fibers, association fibers and commissural fibers – based on location and function. These groups are bunches of fiber tracts travelling along different pathways and connecting to different regions. Therefore, they can be more finely divided into smaller bundles that go in similar directions and serve similar functions. The study of specific tracts can lead to a deeper understanding of their functions.

In 1827, Robert Brown discovered the motion of particles in liquid or gas, known as Brownian motion. In 1905 Einstein published 'Investigations on the Theory of the Brownian Movement' and proposed an equation to measure the diffusivity of molecules under free conditions. Diffusivity can be affected by such factors as temperature, the viscosity of the medium, and molecular size. Isotropic diffusion is found in a homogenous environment, which means that water molecules move randomly, and their displacement demonstrates a Gaussian distribution that always follows Einstein's mathematical description of Brownian motion. However, free diffusion is hindered or restricted under heterogeneous circumstances, which means that water molecules no longer move in random directions, resulting in anisotropic diffusion.

Due to tissue heterogeneity in the brain, such as myelinated axons as a major constraint, the diffusion of water molecules is unlikely to be isotropic. According to Douek (Douek et al., 1991), the diffusion of water molecules is faster in directions parallel to white matter fibers and slower in directions perpendicular to them, and therefore anisotropic. Diffusion-weighted imaging (DWI) allows for the measurement of diffusion and can be used as an indirect measurement of structural parameters.

In 1965, pulsed gradients were introduced into the basic spin echo sequence by Stejskal and Tanner. With the insertion of Stejskal–Tanner formula, an improved system that correlated the diffusion coefficient with the nuclear magnetic resonance (NMR) signal was established with a much higher sensitivity to accommodate the diffusion effect. This was the first time diffusion-weighted sequences were properly described. DWI works by using water molecules as a tracer and measuring its diffusion parameters in diffusion directions. With the development of echo-planar imaging (EPI) in the 1990s, which is faster and solves the problem of motion artifacts, DWI was established for clinical imaging.

Diffusion is a three-dimensional phenomenon and can be influenced by many factors in a microstructural environment, thus behaving differently when parallel or perpendicular to fiber tracts. Therefore, the directionality and orientation of fiber tracts can be traced, and the visualization quantification of white matter fiber tracts are made possible based on this principle. 1994, Peter Basser first proposed the use of diffusion tensor imaging (DTI), which made the description of anisotropic diffusion of water molecules possible (Basser et al., 1994a).

1.2 Diffusion models based on Gaussian distribution and limitations

DWI allows the visualization of water diffusion in a particular direction. Prior to measuring anisotropic diffusion, determining the orientation of axons was essential. Therefore, a tensor formalism that depicted fiber tract orientation was needed. DTI is the most commonly used model that allows a description of the diffusion parameters based on a Gaussian distribution. It is a 3×3 covariance matrix. At least six diffusion measures are necessary to construct the tensor mathematically, and the diffusion parameters are defined as three eigenvectors and three eigenvalues. The three eigenvectors are orthogonal to each other, and eigenvalues represent diffusivity along these three eigenvectors. With three eigenvectors and three eigenvalues, an ellipsoidal model is

defined. The ellipsoid represents diffusion probability, and a three-dimensional tensor model is estimated in which the principal eigenvector is regarded as being along the axis of fiber tracts. This tensor illustrates anisotropic diffusion and is often interpreted as the presence of an axon along the tensor orientation. Information stored in DTI is usually represented as simpler scalar maps. The frequently used parameters of DTI are fractional anisotropy (FA) and mean diffusivity (MD). MD is a parameter that measures average diffusion properties, or in other words, the average of eigenvalues over three orthogonal directions. FA is calculated based on the equation described by Basser and Pierpaoli (Koay et al., 2006) as follows: $\mathrm{FA} = \sqrt{\frac{(\lambda_1 - \mathrm{MD})^2 + (\lambda_2 - \mathrm{MD})^2 + (\lambda_3 - \mathrm{MD})^2}{2({\lambda_1}^2 + {\lambda_2}^2 + {\lambda_3}^2)}}$. As FA and MD are well-established diffusion-tensor-based metrics known to describe a Gaussian distribution of water molecules and represent diffusion capability, they are often used to evaluate asymmetry in microstructures (Basser et al., 1994b).

Tractography can be performed based on DTI data to achieve the three-dimensional reconstruction of fiber tracts. The principal eigenvector suggests that the fiber tracts are heading in one particular direction, and by following the direction of the principal eigenvector successively, a long connection between one part of the brain and another is visualized.

With its feasibility in probing microstructure, DTI is routinely applied in clinical practice as well as research. DTI has been implemented in numerous studies for its capability to detect abnormalities in white matter that might not be visible on conventional magnetic resonance imaging (MRI). This includes neurological diseases like multiple sclerosis (Inglese and Bester, 2010), lateralization (Barrick et al., 2007; Sreedharan et al., 2015), aging and development (Falangola et al., 2008), psychiatry diseases like autism (Kubicki et al., 2007), and others.

Although a deeper, profound understanding of the brain has been achieved thanks to DTI – based as it is on the premise of Gaussian distribution – it is not without limitations (Chanraud et al., 2010). As Gaussian distribution is assumed in a homogeneous medium and describes the normative distribution of a given population, it can be problematic in

such a complex biological environment as the brain. Heterogeneity of the microstructural environment can cause deviation from a Gaussian distribution. Assuming there can only be one single fiber population within one voxel is an unavoidable limitation of DTI. In fact, about one third of the image voxels in the brain contain multiple fibers (Behrens et al., 2007). Based on this single fiber assumption, errors occur in voxels with multiple fiber populations, and false connections might be presented.

But the diffusion tensor model is just one possible model to describe the diffusion in a given voxel. There are also other models. Le Bihan proposed the concept of intra-voxel incoherent motions, in which he illustrated the incapability of the monoexponential model to conclude various types of diffusions of components in the human body, such as perfusion and diffusion, and therefore established a biexponential model (Le Bihan et al., 1986). In this model, he took a step forward and found that the quality of an image was more determined by perfusion when the b value was low, while the effect of true diffusion of water molecules was more significant when the b value was high (Le Bihan et al., 1988). Because the components in the human body are so complex, even the biexponential model failed to meet the requirements. Consequently, Yablonskiy proposed another model, called the stretched exponential (Yablonskiy et al., 2003). These three models are all based on the same premise that diffusion in the human body follows Gaussian diffusion, thus the inability to resolve multiple diffusion directions is inherent to models based on Gaussian distribution.

1.3 Diffusion Kurtosis and model-independent extensions of diffusion-weighted imaging

There are other extensions of DWI that try to solve the problem of multidirectional diffusion.

Diffusion spectrum imaging (DSI), or q-space imaging, is a model-independent method that attempts to solve the fiber crossing confoundment without the need to assume a single diffusion direction (Tuch et al., 2003). With this method, direct measurement of the three-

dimensional diffusion function within each voxel becomes possible because the diffusion signal is converted into a diffusion function by Fourier transformation. But it cannot avoid two limitations. One is that Fourier transformation requires a very short duration time and high gradient amplitude – for the acquisition of an accurate Brownian displacement – of which many clinical MRI scanners are incapable. The other is that a large amount of data is needed for DSI, therefore considerably increasing acquisition time.

Q-ball imaging (QBI) is more efficient than DSI and was designed to overcome the time-consuming disadvantage of DSI while still maintaining the capability to probe microstructure without modelling. Compared to DSI sampling q-space on a complete three-dimensional q-space trajectory, QBI converts q-space to a sphere with sufficient diameter, which is termed a q-ball. These q-balls are models of diffusion density in many orientations, and their peaks are interpreted as the presence of fibers. This is also true for fiber crossings, where q-balls can adequately represent two or more preferential diffusion orientations. However, diffusion density models such as q-balls are inflated relative to underlying anatomical fiber tracts. The idea is that every voxel's diffusion orientation density is comprised of signals originating from one or more fiber tract(s) at different orientations and scales. Problematically, these inflated models are poor at distinguishing fiber tracts crossing at close angles. This situation can cause errors when determining where axons are, for example, estimating two separate tracts into one single bundle. To improve this, fiber orientation density is measured, instead of diffusion orientation density, as it is less likely to suffer from inflated models.

Due to the complexity of intracellular and extracellular environments such as myelin sheaths and organelles, brain tissue is far from an ideal example of homogenous liquid. Gaussian distribution is therefore not in accordance with realistic situations, indicating that a displacement of probability diffusions can appear, and diffusion can consequently deviate from a Gaussian form (Karger, 1985), whereas non-Gaussian distribution is more likely to occur in biological tissue (Tuch et al., 2003).

Compared with the above techniques, the concept of diffusion kurtosis imaging (DKI)

was originally proposed by Jensen in 2005, which quantifies deviation from Gaussian behavior by applying a dimensionless metric called excess kurtosis (Jensen et al., 2005b). Kurtosis is used to show how peaky this distribution is, and it reflects heterogeneity in the tissue environment. The relationship between DTI and DKI is shown as $\ln[S(b)] = \ln[S(0)] - bD_{\mathrm{app}} + \frac{1}{6}b^2D_{\mathrm{app}}^2K_{\mathrm{app}} + \mathrm{O}(b^3)$, where D_{app} and K_{app} mean apparent diffusion coefficient and apparent diffusional kurtosis, respectively. It takes one step further based on the DTI model; it still does an adequate job even though DTI is unable to demonstrate finer connections. With an additional, modestly increased b value, the excess diffusional kurtosis can be approximately determined and thus enable convenient clinical use. Accordingly, about 2000 s/mm^2 is needed for the maximum additional b value besides the normally used b values 0 s/mm^2 and 1000 s/mm^2 in DTI. Furthermore, the DKI model is found to be capable of resolving fiber crossings by calculating orientation distribution function (ODF) based on diffusion kurtosis approximation of the diffusion signal (Lazar et al., 2008).

Instead of seeking to estimate the full diffusion displacement probability distribution, DKI estimates only the kurtosis in addition to other diffusion coefficients. DKI is not as demanding in scanning time and gradient strength as DSI and QBI, which enables the application of DKI to the clinical routine.

1.4 Objectives of the study

DTI has been widely used to study the integrity of white matter tracts of healthy brains as well as various neurological disorders. On the one hand, enormous studies on interhemispheric asymmetry using DTI have been reported on both healthy people (Buchel et al., 2004; Park et al., 2004; Wilde et al., 2009) and patients with neurological dysfunction (Park et al., 2004; Zhou et al., 2018). Various regions have been found to present interhemispheric asymmetry under physiological or pathological conditions. However, image voxels in these regions are likely to contain multiple fibers – and DTI is incapable of resolving crossing or kissing fibers within one voxel. As a result, regions

with dense fiber populations previously found to demonstrate interhemispheric asymmetry might not have actually done so. On the other hand, lesions of white matter in the brain can result in microscopic changes in structure as well as affect surrounding regions. Water molecules in these regions are inevitably affected by pathological changes. In order to probe heterogeneous microstructure, a technique with higher sensitivity than DTI is needed. DKI, as an extension of DTI, characterizes the non-Gaussian random motion of water molecules (Jensen and Helpern, 2010). It has been mostly used for glioma grading. Histograms based on DKI differed significantly between grade II and grade III glioma (Delgado et al., 2017), and DKI also demonstrated feasibility in differentiating low-grade (grade II) from high-grade (grade III and IV) gliomas (Van Cauter et al., 2012; Bai et al., 2016; Falk Delgado et al., 2018). Much less effort is invested in detecting the status of fiber tracts with important functions, such as corticospinal tract (CST) and arcuate fasciculus (AF), which are correlated with patients' prognosis and quality of life. As DKI has proved its feasibility regarding glioma, it may also be effective in detecting changes in CST and AF on glioma patients.

The application of DKI to either healthy volunteers or glioma patients has not been fully explored. To the best of our knowledge, DKI has not yet been utilized in detecting interhemispheric asymmetry using tract-based spatial statistics (TBSS), neither has its potential predictive value for outcomes of hemiparesis and aphasia in high-grade glioma patients been evaluated. With the advantage of increased sensitivity to microstructure as compared to DTI, DKI could also be implemented in research on the topics of white matter mentioned above.

In order to explore the advanced application of DKI, our study is divided into two parts, the application of DKI in interhemispheric asymmetry and the application of DKI in high-grade glioma, respectively.

1.4.1 Application of DKI in interhemispheric asymmetry

Even though both hemispheres of the brain share a similar appearance, they are actually

asymmetrical. But it was not until the 19th century that the direct evidence of this was found by Broca and Wernicke after noticing that speech deficits were more likely to occur with damage to the left hemisphere of the brain. In the 1960s, a group of patients underwent forebrain commissure resections in order to cure epilepsy, and this opened up the possibility for researchers to analyze functions of the cerebral hemispheres independently. More and more functions related to either the left or the right hemispheres were reported in unilateral brain injury cases. Afterwards, the split-brain operation was made possible with drugs and surgery in order to achieve a deeper understanding of cerebral asymmetry.

With the development of technology, evidence for cerebral asymmetry is now more focused on brain imaging. To date, hemispheric dominance is reported by previous studies to correlate with various functions. For example, visual–spatial processing was dominated by the right hemisphere for most people (Vogel et al., 2003), and language processing dominated by the left hemisphere (Bethmann et al., 2007). Many regions that revealed so-called structural interhemispheric asymmetry have also been reported, mostly the left occipital (Chiu and Damasio, 1980), right frontal (LeMay, 1977), and left planum temporale regions (Shapleske et al., 1999). This problem was traditionally addressed by detecting volumes or shapes of specific regions the brain's grey matter by researchers (Luders et al., 2004).

By now, neuroanatomical asymmetry has long been reported to be associated with functional lateralization, not only in the grey matter (Amunts et al., 2000; Toga and Thompson, 2003) but also in the white matter that connects the hemispheres (Beaton, 1997), especially based on the detection from DTI (Buchel et al., 2004; Park et al., 2004; Takao et al., 2011; Shu et al., 2015; Angstmann et al., 2016; Gomez-Gastiasoro et al., 2019).

About a decade ago, the correlation between asymmetry of white matter fibers and behavioral lateralization was less known, contrary to specific regions of the brain. It was not until 2007 that Barrick and his colleagues detected two asymmetric white matter

pathways based on DTI for the first time (Barrick et al., 2007). Since then, several studies have investigated the interaction between handedness and asymmetry in specific fiber tracts, such as the corticospinal tract (Westerhausen et al., 2007; Li et al., 2010; Seizeur et al., 2014) and cingulum bundle (Gong et al., 2005a). White matter asymmetry was not only found in healthy human brains (Cao et al., 2003; Glasser and Rilling, 2008; Thiebaut de Schotten et al., 2011), but also in brains burdened by neurological disorder (Kubicki et al., 2002; Wang et al., 2004).

Some factors like aging and gender have also been reported to affect lateralization (Kansaku et al., 2000; Yu et al., 2014; Agcaoglu et al., 2015), but other studies showed these findings controversial (Gong et al., 2005b; Westerhausen et al., 2007; Takao et al., 2011).

Based on previous studies, the CST, cingulum bundle (CB), inferior fronto-occipital fasciculus (IFOF), inferior and superior longitudinal fasciculus (ILF and SLF), corpus callosum, and the uncinate fasciculus (UF) are the most popular targets for research on white matter asymmetry. Therefore, all these pathways were analyzed in the first part of this study in order to determine the asymmetric white matter regions in healthy subjects. The anterior thalamic radiation (ATR), as one of the largest fiber tracts in the white matter, was also analyzed because few studies have looked into asymmetry in this fiber bundle. The application of DKI to detecting interhemispheric asymmetry was performed using TBSS on both DTI- and DKI-based parametric maps. TBSS analysis allows DTI- and DKI-based parametric maps to be directly compared and their performances in detecting interhemispheric asymmetry to be evaluated. Factors like handedness and gender were also evaluated for their effect on interhemispheric asymmetry.

1.4.2 Application of DKI in glioma

Gliomas are the most frequent brain malignancies and account for 70% of malignant primary brain tumors in adults, of which the annual incidence is six cases per 100,000. Among them, grade III and IV gliomas are regarded as high-grade gliomas. Median

survival for patients with grade III astrocytoma was expected to be three years in one study (Keles et al., 2006) and 24 months in another (Dong et al., 2016), respectively, while that of glioblastoma was reported to be only 15 months with a combination of temozolomide and radiotherapy (Stupp et al., 2009). Neither of these components of high-grade glioma has shown satisfactory overall survival. But in other studies, 416 patients with primary or recurrent glioblastoma were reported to benefit from the extent of resection (EOR), and overall survival was extended by 4.2 months (Yong and Lonser, 2011). In another study, mean survival for 135 glioblastoma patients with EOR ≥ 98% was 14 months compared to 9 months with EOR < 98% (Kuhnt et al., 2011). EOR was found to be correlated with a better outcome in glioma patients (Pope and Brandal, 2018). The health-related quality of life for glioma patients can also be improved by surgery (Dirven et al., 2014).

But EOR in areas involved with functional tracts like the CST and AF remains a great challenge to neurosurgeons in the uncertainty of predicting postoperative motor or language function. Though the use of a gadolinium-based contrast agent in T1 contrast-enhanced imaging greatly assists in detecting the assumed boundaries of a tumor with a compromised blood–brain barrier, it does not aim at measuring tumor activity specifically. To make up for the limitation on conventional MRI techniques, such as T1 contrast-enhanced images, more advanced MRI techniques are needed. For example, DWI is often applied as a complementary tool because changes in cellular density due to the presence of a tumor or neoplasm can also change the diffusion of water molecules, especially in patients with high-grade glioma (Dhermain et al., 2010; Pope and Brandal, 2018). In the microstructural environment, a tumor core with increased cellularity results in a more limited extra-cellular space that presents a lower apparent diffusion coefficient (ADC); consequently, ADC reflects cellularity indirectly.

To lessen the tumor burden, as well as to preserve vital functions, is the goal of modern glioma surgery. Even grossly abnormal-appearing fibers in tumor masses were found to retain functionality to some extent through intraoperative subcortical mapping (Ojemann

et al., 1996; Bello et al., 2008). Preoperative visual assessment for predicting function preservation is far from reliable, yet a relatively convincing prognosis of motor and language deficits must still be made in order to decide on the best surgical strategy.

It is not uncommon that both lesion size and lesion location were found to relate to impairment, and lesions on motor-related regions such as the primary motor areas, corona radiata, and internal capsule can affect the possibility of motor function recovery. But lesion load (tract–lesion overlap volume) on CST was a more direct predictor of motor deficit in chronic stroke (Zhu et al., 2010), and in another study, lesion load on CST was able to predict stroke patients' motor outcomes at three months (Feng et al., 2015). Likewise, lesion load on the left AF was found to potentially predict language impairment and recovery outcomes to some extent (Marchina et al., 2011). Other methods, like motor-evoked potentials (MEPs) (Catano et al., 1996) and functional magnetic resonance imaging (fMRI) (Ward et al., 2006), have also been tried. But MEPs showed a lack of specificity because their absence did not necessarily correlate with poor recovery (Arac et al., 1994), and fMRI was impractical because patients had to be able to follow instructions during scanning, which was not always feasible. But combing intraoperative fMRI and DTI can be of great help in achieving maximum resection while maintaining the neurological function of the brain, according to another study (Nimsky, 2011). DTI has been implemented to predict motor recovery and CST damage at the level of the posterior limb of the internal capsule (PLIC) and has significantly predicted unfavorable motor outcome (Puig et al., 2011). In glioma patients, the level of injury to the CST, quantified by measuring FA on PLIC bilaterally, has been reported to be able to assess lesion and tumor infiltration areas on CST (Gao et al., 2017). DTI has also been applied in detecting the level of intactness of white matter fiber tracts and visualizing their relative locations to brain lesions, especially in preoperative assessments intended to preserve vital functions of fiber tracts (Farshidfar et al., 2014; Caverzasi et al., 2016; Dubey et al., 2018), because the spared functional regions improve the quality of life for patients. Several studies have applied DKI in glioma grading (Van Cauter et al., 2012; Jiang et al.,

2015; Delgado et al., 2017), and high kurtosis was found to correlate with high cellularity, as well as high eccentricity (Szczepankiewicz et al., 2016). Others have also found that MK could serve as a biomarker for predicting outcomes of high-grade glioma patients in terms of survival (Wang et al., 2019). Analyses of histograms based on DKI have been performed to evaluate glioma cases preoperatively, due to its capability to reflect the complexity and heterogeneity of microstructures (Qi et al., 2018). But to the best of our knowledge, studies using DKI to evaluate the integrity of fiber tracts in glioma patients are rare, despite its feasibility.

A deeper understanding of the relationships between lesions on both fiber tracts (CST and AF) and motor and language deficits is required. In the second part of the current study, templates of CST and AF were created based on parametric maps of DKI and DTI data from healthy volunteers in order to visualize abnormal locations of the CST and AF in patients not only in glioma-affected areas but also in regions that were distant from the tumor. This method thus reveals the potential prognostic value of DKI- and DTI-derived parameters in the recovery outcome for patients with high-grade glioma in a retrospective study and has expanded the advanced application of DKI.

2 Materials and Methods

Part 1: DKI in Interhemispheric Asymmetry

2.1 Subjects

This retrospective project was approved by the ethics committee at the Philipps University of Marburg in Germany (study 9/13) based on the Declaration of Helsinki. Twenty healthy volunteers were recruited for this study, including 10 males and 10 females (males: 23–32 years, mean age 25 ± 2.6 years; females: 22–26 years, mean age 24 ± 1.2 years). Volunteers' handedness measurements were obtained using the Edinburgh handedness scale (left-handed: 3; right-handed: 17). None of the healthy volunteers suffered from neurological diseases, psychiatric disorders, significant brain injuries, or other known diseases, and none of them were reported to suffer from alcohol dependence or take medication with known effects that would interfere with the study.

2.2 MRI data acquisition

Image acquisition was performed using a 3 Tesla Siemens MRI scanner (Trio, Siemens, Erlangen, Germany) using a 12-multichannel receiver head coil. Participants' assumption of the supine position was required, and their heads were fixed with soft foam rubber pads to minimize head bulk motion.

Diffusion-weighted images were acquired by applying single-shot echo-planar imaging sequences with the following settings: slice thickness 2 mm, field of view (FoV) 256×256 mm^2， matrix 128×128, 60 axial slices without slice gap, repetition time (TR) 8500 ms, echo time (TE) 101 ms, phase encoding direction anterior >> posterior, b-values 0, 1000, and 2000 s/mm^2 respectively, 30 non-collinear diffusion encoding directions, bandwidth 1502 Hz, and phase partial Fourier 6/8. All image sets were visually inspected for severe artifacts and were excluded from the study if any occurred. No severe artifacts were seen.

2.3 Post-processing of MRI data

DWI data was processed using FSL 6.01 (FMRIB Software Library, Oxford, United Kingdom, http://www.fmrib.ox.ac.jk/fsl), in which DWI images were corrected for head motion and eddy currents (Smith et al., 2004; Woolrich et al., 2009) using the 'eddy_openmp' tool. Brain extraction was achieved using the 'BET' tool.

After correction and brain extraction, DWI data were loaded as single 4D NifTI images with the gradient sampling files into the in-house software package Diffusion Kurtosis Estimator (http://nitrc.org/projects/dke), applying the standard protocol (Tabesh et al., 2011). During this process, both DTI processing and DKI processing were selected with 'Advanced Function' to enable the DTI model-fitting method and DKI model-fitting method. Maps of diffusion-tensor-based parameters (DTI_FA, DTI_MD) and maps of diffusion-kurtosis-based parameters (DKI_FA, DKI_MD, DKI_MK) were estimated, allowing for DTI and DKI analysis.

2.4 Tract-based spatial statistics (TBSS) analysis

2.4.1 TBSS for interhemispheric asymmetry on parametric maps

Derived parametric maps (DTI_FA, DTI_MD, DKI_FA, DKI_MD, DKI_MK) were processed using TBSS in FSL (FMRIB Software Library 6.0, Oxford, United Kingdom, https://fsl.fmrib.ox.ac.uk/fsl/fslwiki/) (Smith et al., 2006).

First, all DTI_FA data were aligned with FMRIB58_FA into the standard 1x1x1 mm^3 MNI152 space using non-linear registration. Second, mean DTI_FA data was created and skeletonized using a threshold of FA > 0.2 for the mean DTI_FA skeleton image. Finally, based on this original mean DTI_FA skeleton, a symmetric mean DTI_FA skeleton was derived using 'tbss_sym'. In this step, the pre-aligned DTI_FA datasets were left–right flipped (DTI_FA_flipped), and the flipped DTI_FA data was subtracted from the original non-flipped DTI_FA images. After subtraction, the resulting image was divided into left and the right halves separated along the midsagittal plane. In order to test leftward

asymmetry (left > right), a generalized linear model (GLM) was set up using the 'FSL Randomize' tool. To test for rightward asymmetry (right > left), a GLM was likewise set up.

DKI_FA data was processed using the same protocol. Other maps such as DTI_MD, DKI_MD, and DKI_MK were projected onto the corresponding FA skeleton.

To test for interhemispheric differences in relation to handedness and gender, the GLM was adapted accordingly using the 'FSL Randomize' tool (Nichols and Holmes, 2002; Winkler et al., 2014). The number of permutations was set to 5,000, and threshold-free cluster enhancement was used for correction. The threshold for statistical significance was set to $p < 0.05$.

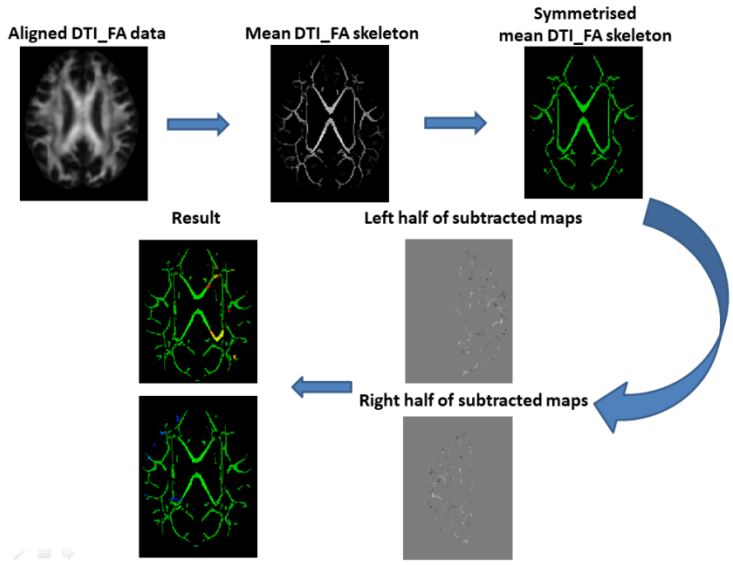

Figure 1. Workflow of dataset preparation for interhemispheric asymmetries

2.4.2 Comparison between DTI- and DKI-based parameters

2.4.2.1 Comparison between DTI_FA and DKI_FA

Both maps of DTI_FA and DKI_FA were loaded into FSL. First, both datasets were aligned with FMRIB58_FA into the standard 1x1x1 mm^3 MNI152 space using non-linear registration. Second, mean FA data was created and skeletonized with a threshold of FA > 0.2. Finally, all images from both groups were projected onto the mean FA skeleton.

Voxel-wise analysis was then carried out. The number of permutations was set to 5,000, and a threshold-free cluster enhancement was used for correction. The threshold for statistical significance was set to $p < 0.05$.

2.4.2.2 Comparison between DTI_MD and DKI_MD

In order to perform a comparison between DTI_MD and DKI_MD, maps of DTI_FA, DTI_MD, DKI_FA and DKI_MD were loaded into FSL. First, DTI_FA and DKI_FA were aligned with FMRIB58_FA into the standard 1x1x1 mm^3 MNI152 space using non-linear registration. Second, mean FA data was created and skeletonized with a threshold of FA > 0.2. In this step, the mean FA skeleton was created. Then, both DTI_MD and DKI_MD were projected onto the mean FA skeleton. Finally, voxel-wise analysis was carried out. The number of permutations was set to 5,000 and threshold-free cluster enhancement was used for correction. The threshold for statistical significance was set to $p < 0.05$.

2.5 Asymmetry of fiber tracts and laterality

In order to visualize asymmetry of the fiber tracts, statistically significant clusters from TBSS analysis were labelled on nine major fiber bundles (CST, Fmi, Fma, IFOF, ILF, SLF, CB, UF, and ATR) by using the Johns Hopkins University (JHU) white matter tractography atlas (Wakana et al., 2007; Hua et al., 2008) and thickened for better visualization using 'tbss_fill' in FSL.

Laterality index (LI) was calculated to test whether all nine major fiber tracts in all right-handed volunteers were leftward dominant, as well as to perform a direct comparison of significant clusters' size of fiber tracts on both hemispheres that may contribute to lateralization. LI was calculated using $(A_L-A_R)/(A_L+A_R)$ (Binder et al., 1996), where A_L represents all statistically significant clusters of TBSS analysis in the left hemisphere and A_R in the right hemisphere. A positive value obtained from this equation indicates leftward dominance, while a negative value suggests rightward dominance.

Part 2: DKI in Glioma Patients

2.6 Subjects

This retrospective project was approved by the ethics committee at the Philipps University of Marburg in Germany (study 9/13), based on the Declaration of Helsinki. Data of healthy volunteers was a subset of the data from Part 1, in which only the right-handed volunteers were included, because 95% of the right-handers and 85% of left-handers showed leftward language lateralization (Pujol et al., 1999; Lurito and Dzemidzic, 2001). Patient data was obtained during the clinical routine.

2.6.1 Healthy volunteers

The current study included 17 healthy right-handed volunteers – nine males and eight females (males: 22–32 years, mean age 25 ± 2.8 years; females: 22–26 years, mean age 24 ± 1.4 years). None of the healthy volunteers suffered from neurological disease, psychiatric disorder, significant brain injury, or other known diseases. None of the volunteers was reported to suffer from alcohol dependence or take medication with known effects that would interfere with our study.

2.6.2 Patients with high-grade glioma

Thirteen right-handed high-grade glioma patients, 12 males and one female (41–70 years, mean age 55 ± 10.7 years) diagnosed with anaplastic astrocytoma WHO III (n = 3), anaplastic oligodendroglioma WHO III (n = 2), anaplastic glial tumor WHO III (n = 1), glioblastoma WHO IV (n = 3), recurrent glioblastoma WHO IV (n = 4) were recruited for this study. Clinical symptoms (hemiparesis and aphasia) of patients preoperative (interval: 0–1 day) and postoperative (interval: 93–1,540 days, mean 657 ± 487 days) were observed and recorded.

2.7 MRI data acquisition

Image acquisition was performed using a 3 Tesla Siemens MRI scanner (Trio, Siemens, Erlangen, Germany) with a 12-multichannel receiver head coil. Patients were required to assume the supine position, and their heads were fixed with soft foam rubber pads to minimize head bulk motion.

Diffusion-weighted images were acquired by applying single-shot echo-planar imaging sequence with the following settings: slice thickness 2 mm, FoV 256×256 mm^2， matrix 128×128, 60 axial slices without slice gap, TR 8500 ms, TE 101 ms, phase encoding direction anterior >> posterior, b-values 0, 1000, 2000 s/mm^2 respectively, 30 non-collinear diffusion encoding directions, bandwidth 1502 Hz, and phase partial Fourier 6/8.

T1-weighted images were acquired by applying a rapid gradient echo sequence with following settings: slice thickness 1 mm, FoV 256×256 mm^2, matrix 128×128, 176 slices, TR 1900 ms, TE 2.26 ms, and bandwidth 199 Hz.

T2 weighted images were acquired by applying single-shot echo-planar sequence with following settings: slice thickness 1 mm, FoV 256×256 mm^2, matrix 128×128, 176 slices, TR 3200 ms, TE 402 ms, and bandwidth 751 Hz.

All image sets were visually inspected for severe artifacts and were excluded if any occurred. No severe artifacts were seen.

2.8 Post-processing of MRI data

DWI data was processed using FSL 6.01 (FMRIB Software Library, Oxford, United Kingdom, http://www.fmrib.ox.ac.jk/fsl) in which DWI images were corrected for head motion and eddy currents (Smith et al., 2004; Woolrich et al., 2009) using the ‘eddy_openmp’ tool. Brain extraction was achieved using the ‘BET’ tool.

After correction and brain extraction, DWI data was loaded as single 4D NifTI images with the gradient sampling files loaded into the in-house software package Diffusion Kurtosis Estimator (http://nitrc.org/projects/dke) applying standard protocol (Tabesh et al., 2011) in order to estimate the diffusion kurtosis and to calculate DKI-based parametric

maps.

In the meantime, DWI data was loaded as single 4D NifTI images and fed into the diffusion spectrum imaging studio (DSI studio; http://dsi-studio.labsolver.org) including b vectors and b values. After image loading, a brain mask was set up automatically to filter out the background region and guarantee efficacy (see Figure 2). Images loaded in DSI studio were automatically normalized in MNI space by the q-space diffeomorphic reconstruction (QSDR) (Yeh and Tseng, 2011). DTI_FA and DTI_MD maps were derived based on the DTI fitting method. T1-weighted images and DKI_MK maps were registered to the derived DTI_FA map using rigid-body registration.

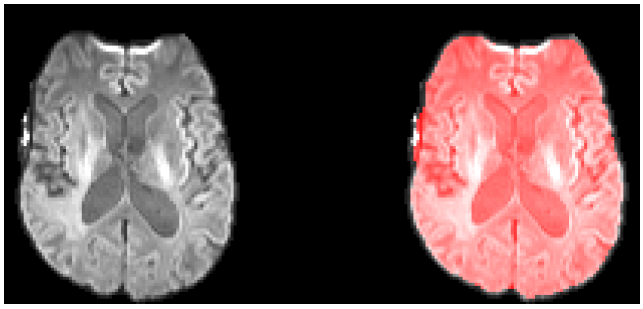

Figure 2. Brain mask for loaded image

2.9 Fiber tractography of the CST and AF

For fiber tractography of the CST and AF, the precentral gyrus, the cerebral peduncle, Broca's area (Brodmann areas 44 and 45), and Wernicke's area (Brodmann area 22) were assigned as regions of interest (ROI) based on atlases in DSI studio. ROIs were then adjusted manually and modified to suit anatomical positions in T1-weighted images for both healthy volunteers and patients. The input tract count was set to 10,000 to guarantee adequate targeting of tracts for analysis. Reconstructed tracts were then automatically recognized and clustered using the 'recognizing and clustering' function. Every derived trajectory was carefully inspected, compared with anatomical positions on the T1-weighted images, and edited manually to achieve a more precise reconstruction.

2.10 Template creation

DTI_FA, DTI_MD, and DKI_MK maps from both healthy volunteers and patients were projected onto the reconstructed CST and AF. As the reconstructed CST and AF trajectories were a series of three-dimensional coordinates, projected data of DTI_FA, DTI_MD and DKI_MK mapped onto the CST and AF of both healthy volunteers and patients was averaged along the x, y, and z axes using kernel density estimator, with bandwidth at voxel-sized scales.

Statistics of CST and AF for every healthy volunteer were accumulated and averaged in MATLAB. Mean values and standard deviations (SD) of DTI_FA, DTI_MD, and DKI_MK of both CST and AF were calculated along the x, y, and z axes. In this way, templates of CST and AF on both hemispheres, based on datasets from healthy volunteers, were created for later comparison with patients' datasets.

Both template and patients' datasets were plotted in MATLAB for visualization comparison between patients' datasets and templates. Patient data within the space between the upper threshold (mean + SD) and lower threshold (mean − SD) of templates were considered normal. Patient data that exceeded the upper threshold or fell below the lower threshold of templates were considered increased or decreased, respectively (see Figure 3).

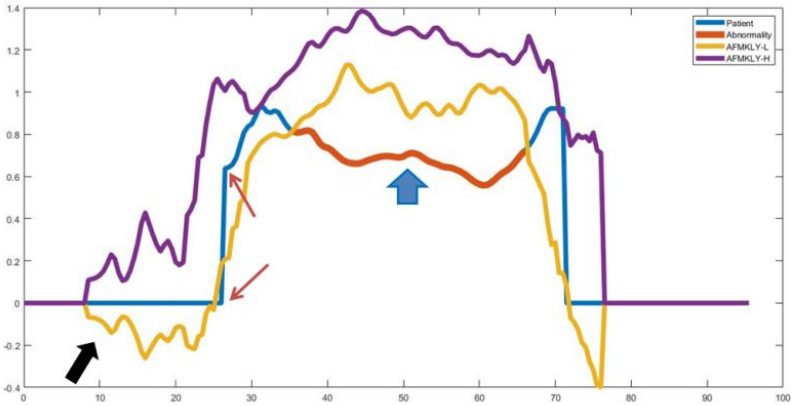

Figure 3. Illustration of AF template based on DKI_MK along y direction.

(Black arrow: value of this part of the curve is below zero, related to the portion of the

template where most variance occurred, red arrow: fiber tract begins at this point, with a sudden change from zero to a non-zero value, blue arrow: abnormal portion of AF because it is lower than mean – SD).

2.11 Detection of the relationship between brain lesion and change on CST and AF

2.11.1 Segmentation of tumor and peritumoral edema

The T2 weighted images from patients were fed into 3D Slicer 4.8.1 for segmentation of the lesions (Kikinis and Pieper, 2011). The premier range of abnormal-appearing regions was roughly delineated and the 'GrowCutEffect' was used to fill the abnormal region. The outlined region was then erased by the 'ChangeLabelEffect', and the region for segmentation was prepared. In this way, the differentiation of normal-appearing brain tissue from possibly abnormal regions was enabled, and abnormal regions with high signal density that indicated tumor tissue and peritumoral edema were selected and segmented according to standard protocol (Kikinis and Pieper, 2011). This semi-automatic segmentation of those regions of the brain possibly affected or infiltrated by glioma was performed in order to reveal their spatial information for analyzing its influence on the reconstructed CST and AF (see Figure 4).

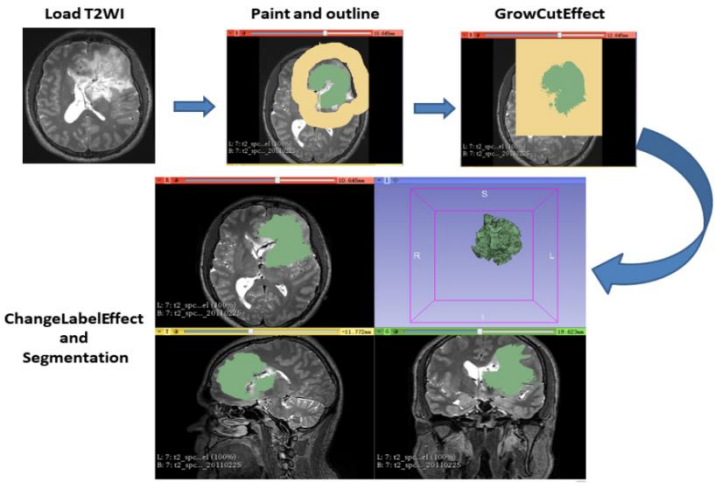

Figure 4. Segmentation procedure

2.11.2 Visualization of change on CST and AF in relation to brain lesion

By comparing the healthy volunteers' CST and AF templates on corresponding slices, the coordinates of changes were recorded and exported from MATLAB. In DSI studio, reconstructed trajectories were cut according to recorded coordinates to achieve visualization of changes on CST and AF. The absolute volumes of changes (FAV, MDV, MKV) on CST and AF, and their percentages of the whole tract (FAV%, MDV%, MKV%) based on DTI_FA, DTI_MD and DKI_MK, were also recorded.

Segmented brain lesions from 3D slicer were loaded into DSI studio. In this way, the spatial relationships between brain lesions and CST and AF changes were inspected.

2.12 Pattern for indication and prediction of motor and language deficits

Potential combinations of change seen in DTI_FA, DTI_MD, and DKI_MK were inspected for all patients.

As change on CST and AF can lead to motor and language dysfunction, combinations of changes of CST or AF were carefully analyzed for possible correlation with preoperative and postoperative persisting or emerging hemiparesis and aphasia. A pattern that matched best might be found by summarizing possible changes on DTI_FA, DTI_MD, and DKI_MK in patients presenting with hemiparesis or aphasia.

In order to determine the predictive capability of the pattern, sensitivity and specificity were calculated for the pattern.

2.13 Statistical analysis

Statistical analysis was conducted using SPSS 22.0. Spearman correlation analysis was used for evaluating the relationship between FAV and MKV, MDV and MKV, FAV% and MKV%, and MDV% and MKV%, respectively. Pearson correlation analysis was used for calculating the correlation between FAV and MDV, and FAV% and MDV%, respectively. The level of significance was set to $p < 0.05$.

3 Results

Part 1: DKI in interhemispheric asymmetry

3.1 Interhemispheric asymmetry

Voxel-wise comparison was performed on the entire brain white matter skeleton in order to acquire interhemispheric asymmetry. Results of both leftward and rightward asymmetries were masked in nine major fiber tracts (CST, Fmi, Fma, IFOF, ILF, SLF, CB, UF, and ATR) as shown in Table 1.

Table 1. Voxel-wise statistical analysis of interhemispheric asymmetry

		MAX t-Value				
		DTI_FA	DTI_MD	DKI_FA	DKI_MD	DKI_MK
CST	L > R	0.981	0.353	0.954	0.054	0
	R > L	0.976	0.875	0.965	0.161	0.853
Fmi	L > R	0.974	0.470	0.958	0.115	0.134
	R > L	0.948	0.786	0.920	0.993	0.464
Fma	L > R	0.982	0.000	0.966	0.000	0.001
	R > L	0.978	0.860	0.929	0.000	0.000
ILF	L > R	0.979	0.591	0.933	0.384	0.414
	R > L	0.978	0.980	0.959	0.555	0.652
IFOF	L > R	0.978	0.952	0.920	0.000	0.638
	R > L	0.978	0.956	0.952	0.105	0.942
SLF	L > R	0.992	0.948	0.933	0.491	0.638
	R > L	0.991	0.799	0.946	0.167	0.842
UF	L > R	0.978	0.948	0.920	0.043	0.638
	R > L	0.957	0.888	0.945	0.000	0.009
CB	L > R	0.982	0.580	0.997	0.993	0.334
	R > L	0.965	0.857	0.929	0.009	0.116
ATR	L > R	0.999	0.905	0.992	0.095	0.977
	R >L	0.998	0.997	0.933	0.006	0.355

In DTI_FA, both leftward and rightward asymmetries were detected in CST (L > R: $p < 0.019$; R > L: $p < 0.024$), Fma (L > R: $p < 0.018$; R > L: $p < 0.022$), ILF (L > R: $p < 0.021$; R > L: $p < 0.022$), IFOF (L > R: $p < 0.022$; R > L: $p < 0.022$), SLF (L > R: $p < 0.009$; R > L: $p < 0.009$), UF (L > R: $p < 0.022$; R > L: $p < 0.043$), CB (L > R: $p < 0.018$; R > L: $p < 0.035$) and ATR (L > R: $p < 0.001$; R > L: $p < 0.002$); except for Fmi, only leftward asymmetry was found (L > R: $p < 0.026$) (see Figure 5).

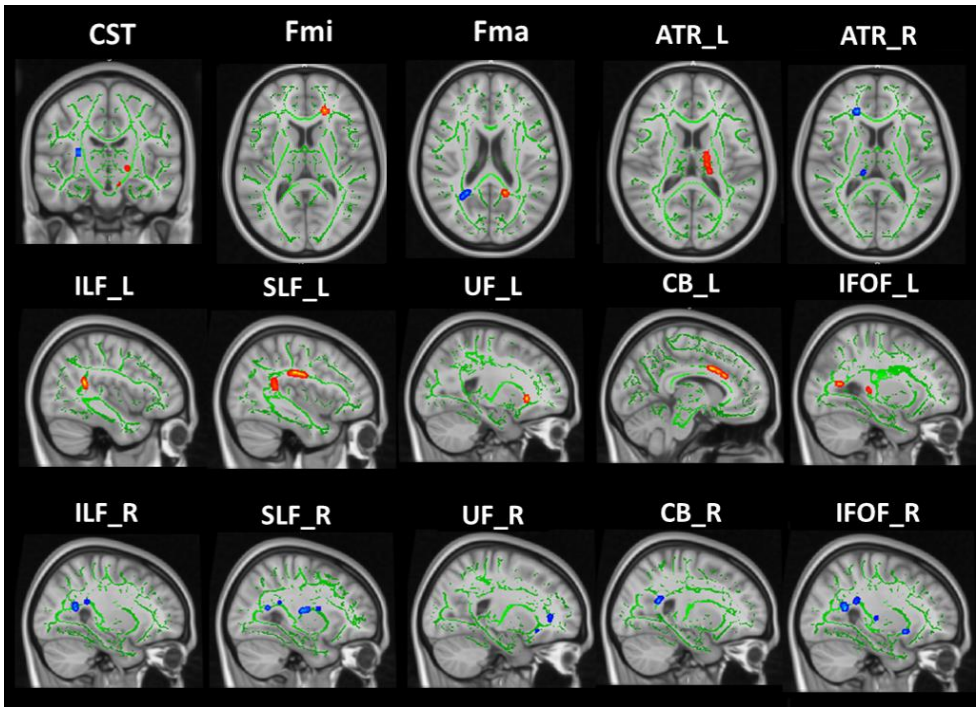

Figure 5. Distribution of statistically significant asymmetric regions (DTI_FA) (green: mean-FA skeleton of healthy volunteers, red: leftward asymmetry, blue: rightward asymmetry)

In DTI_MD, leftward and rightward asymmetries were found in IFOF (L > R: $p < 0.048$; R > L: $p < 0.044$), rightward asymmetry was found in ILF (R > L: $p < 0.020$), and ATR (R > L: $p < 0.003$) (see Figure 6).

In DKI_FA, leftward and rightward asymmetries were found in CST (L > R: $p < 0.046$; R > L: $p < 0.035$). Leftward asymmetry was found in Fmi (L > R: $p < 0.042$), Fma (L >

R: $p < 0.034$), CB (L > R: $p < 0.003$) and ATR (L > R: $p < 0.008$). Rightward asymmetry was found in ILF (R > L: $p < 0.041$) and IFOF (R > L: $p < 0.048$) (see Figure 7).

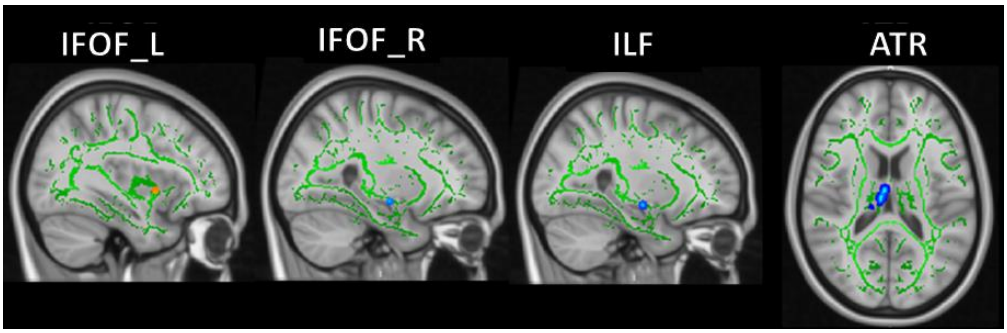

Figure 6. Distribution of statistically significant asymmetric regions (DTI_MD) (green: mean-FA skeleton of healthy volunteers, red: leftward asymmetry, blue: rightward asymmetry)

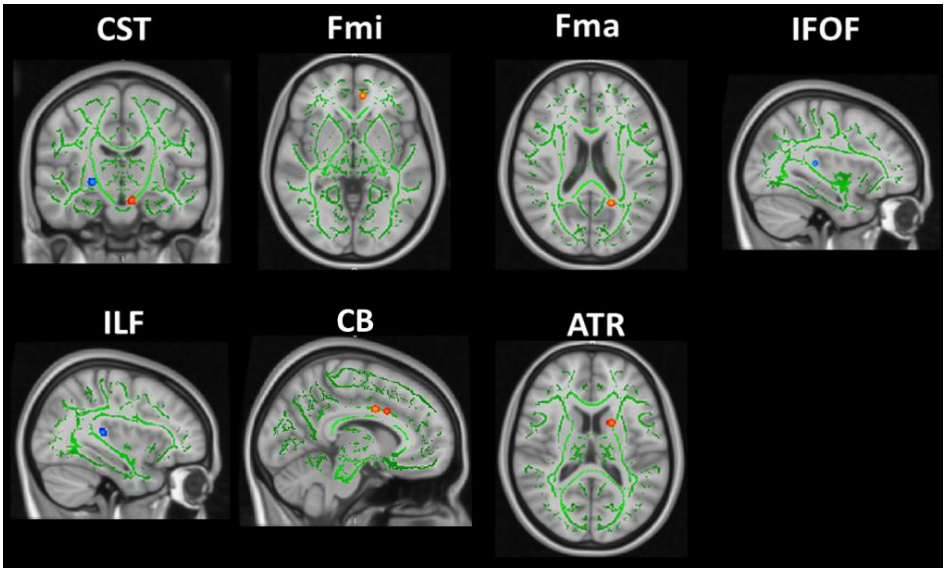

Figure 7. Distribution of statistically significant asymmetric regions (DKI_FA) (green: mean-FA skeleton of healthy volunteers, red: leftward asymmetry, blue: rightward asymmetry)

In DKI_MD, only rightward asymmetry was found in Fmi (R > L: $p < 0.007$), and leftward asymmetry was found in CB (L > R: $p < 0.007$) (see Figure 8).

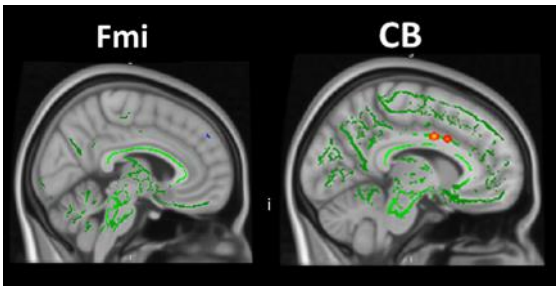

Figure 8. Distribution of statistically significant asymmetric regions (DKI_MD) (green: mean-FA skeleton of healthy volunteers, red: leftward asymmetry, blue: rightward asymmetry)

In DKI_MK, only leftward asymmetry was found in ATR (L > R: $p < 0.023$) (see Figure 9).

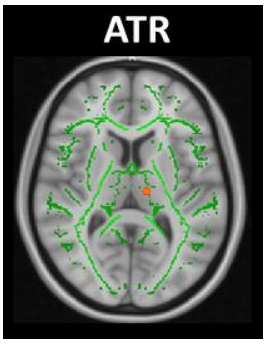

Figure 9. Distribution of statistically significant asymmetric regions (DKI_MK) (green: mean-FA skeleton of healthy volunteers, red: leftward asymmetry)

3.2 Effects of gender and handedness

No significant effect was found for gender and handedness in DTI- and DKI-derived parameters (see Table 2).

Table 2. Voxel-wise statistical analysis for gender and handedness effects

Note: LH: left-handed; RH: right-handed; L: left hemisphere; R: right hemisphere.

		MAX t-Value				
		DTI_FA	DTI_MD	DKI_FA	DKI_MD	DKI_MK
gender	L > R	0.335	0.890	0.605	0.152	0.560
	R > L	0.153	0.946	0.428	0.101	0.923
handedness	LH > RH	0.607	0.071	0.852	0.101	0.497
	RH > LH	0.065	0.811	0.122	0.797	0.136

3.3 Laterality of fiber tracts on DTI- and DTI-based parameters

A LI was calculated for nine major fiber tracts in the DKI_FA and DTI_FA maps of the subgroup of all 17 right-handed volunteers (see Table 3). A LI above zero was considered representative of leftward dominance, which was found in Fmi, Fma, CB, and ATR in DKI_FA; but in DTI_FA, leftward dominance was found in CST, SLF, and CB. However, rightward dominance was found in CST, ILF, IFOF in DKI_FA, and Fmi, Fma, ILF, IFOF, UF, and ATR in DTI_FA. No dominance was found in SLF or UF in DKI_FA. Only dominance in ILF, IFOF, and CB was concurrent in DKI_FA and DTI_FA. Dominance in CST, Fmi, Fma and ATR of DKI_FA contradicted with that in DTI_FA.

In DTI_MD, both leftward and rightward asymmetries found on IFOF were with a cluster size of 1 voxel, and no dominance was found on IFOF. Rightward dominance was found on ILF (3 voxels) and ATR (80 voxels). In DKI_MD, rightward dominance was found on Fmi with a cluster size of 1 voxel, and leftward dominance was found on CB with a cluster size of 4 voxels. In DKI_MK, leftward dominance was found on ATR with a cluster size of 3 voxels.

Table 3. Size of significant clusters and laterality index of fiber tracts based on DKI_FA and DTI_FA

	DKI_FA (#Voxels)		LI	DTI_FA (#Voxels)		LI
	Leftward	Rightward		Leftward	Rightward	
CST	5	7	−0.17	42	5	0.79
Fmi	3	0	1.00	0	74	−1.00
Fma	6	0	1.00	22	55	−0.43
ILF	0	4	−1.00	26	81	−0.51
IFOF	0	1	−1.00	18	55	−0.51
SLF	0	0	0.00	196	18	0.83
UF	0	0	0.00	15	22	−0.19
CB	9	0	1.00	70	27	0.44
ATR	10	0	1.00	98	112	−0.07

3.4 Comparison between DTI- and DKI-based parametric maps

Significant differences were found in 79.06% of the skeletons ($p < 0.0002$) comparing DTI_FA and DKI_FA. Fractional anisotropy was significantly higher in DKI_FA than in the corresponding DTI_FA. No significant cluster was found in which fractional anisotropy in DTI_FA was higher than in the corresponding DKI_FA ($p < 0.331$) (see Figure 10).

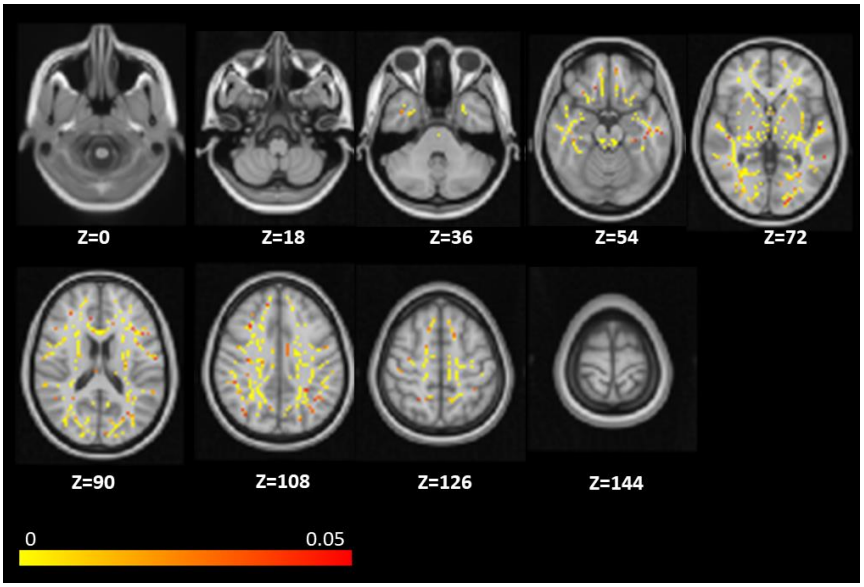

Figure 10. Distribution of significant differences according to DTI_FA and DKI_FA, shown in every 18 slices along the z-axis (p < 0.05, FWE-corrected).

Significant differences were found in 79.06% of the skeletons (p < 0.0002) comparing DTI_MD and DKI_MD. Mean diffusivity was significantly higher in DKI_MD than in the corresponding DTI_MD. No significant cluster was found in which mean diffusivity in DTI_MD was higher than the corresponding DKI_MD (p < 0.331) (see Figure 11).

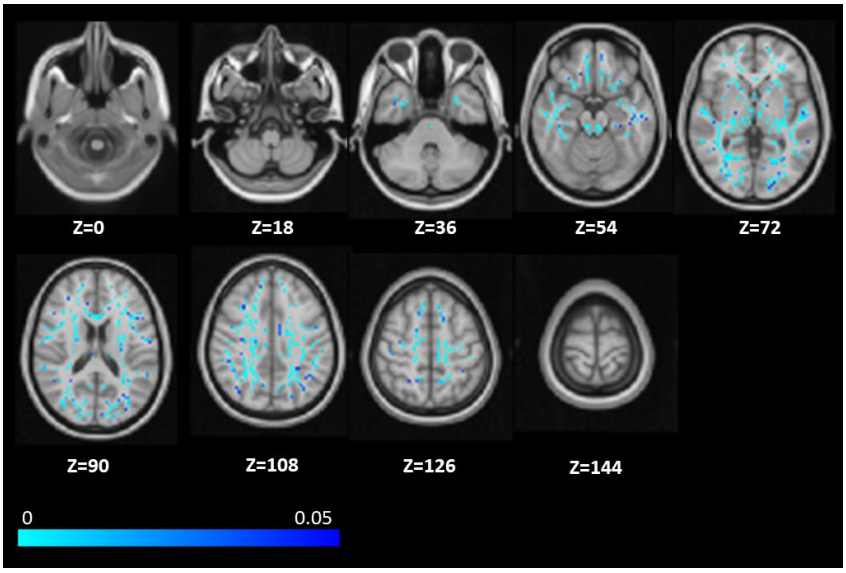

Figure 11. Distribution of significant differences according to DTI_MD and DKI_MK, shown in every 18 slices along the z-axis (p < 0.05, FWE-corrected).

Part 2: DKI in Glioma Patients

3.5 Patients' clinical information

Patients' clinical information was obtained and is listed in Table 4 and 5 Two patients showed hemiparesis preoperatively. One of them was diagnosed with grade III anaplastic oligodendroglioma (patient #1), and the other with grade IV primary glioblastoma (patient#12).

In follow-up records, hemiparesis in patient #1 persisted until the end of observation, and patients #3 and #6 – diagnosed with grade III anaplastic astrocytoma – presented with emerging hemiparesis in the follow-up. Hemiparesis in patients #12 was also persistent; patients #9 and #11 – diagnosed with grade IV primary glioblastoma – and patients #7and #8 – diagnosed with grade IV residual glioblastoma – presented with emerging hemiparesis in the follow-up.

Six patients showed aphasia preoperatively. One of them was diagnosed with grade III anaplastic oligodendroglioma (patient #1), one of them was diagnosed with grade III anaplastic astrocytoma (patients #4) and one with grade III anaplastic glial tumor (patient #2), two of them (patients #7 and #8) were diagnosed with grade IV residual glioblastoma, and one with grade IV primary glioblastoma (patient #9).

In follow-up records, aphasia persisted in patient #1, but gradually alleviated and finally vanished in the two patients with grade III anaplastic astrocytoma (patients #4 and #6) and one with grade III anaplastic glial tumor (patient #2), while aphasia persisted in three patients diagnosed with grade IV glioblastoma, either residual or primary (patients #7, #8, and #9). Another patient diagnosed with grade IV residual glioblastoma presented with emerging aphasia (patient #13) in the follow-up.

The interval of observation ranged from 93 days to 1,540 days; the average interval of observation was thus 657 days. In follow-ups, three changes in clinical symptoms (hemiparesis or aphasia) were found. Hemiparesis or aphasia could be worsened or alleviated and vanished, and previous non-existing symptoms could emerge in the

follow-up.

Table 4. Clinical characteristics of patients

(R: right, L: left, LT: left temporal, LF: left frontal, RC/L: right central/lateral, LTB: left temporal-basal, RT: right temporal, RP: right parietal, RPO: right parietal-occipital, AO: anaplastic oligodendroglioma, AGT anaplastic glial tumor, AA: anaplastic astrocytoma, RG: recurrent glioblastoma, G: glioblastoma.)

Patient	Gender	Age (years)	Handedness	Location	Histopathology
Grade III					
1	M	61	R	LT	AO, WHO III
2	M	65	R	LT	AGT, WHO III
3	M	70	R	LT	AA, WHO III
4	F	53	R	LT	AA, WHO III
5	M	38	R	LF	AO, WHO III
6	M	45	R	RC/L	AA, WHO III
Grade IV					
7	M	41	R	LT	RG, WHO IV
8	M	41	R	LTB	RG, WHO IV
9	M	54	R	LT	G, WHO IV
10	M	62	R	RT	RG, WHO IV
11	M	62	R	RP	G, WHO IV
12	M	66	R	RT	G, WHO IV
13	M	57	R	RPO	RG, WHO IV

Table 5. Neurological characteristics of patients

('+': persisting positive symptom until observation stopped, '−': negative symptom when observation stopped, '±': symptom once appeared but was gradually improved and vanished at the end of observation, 'interval': the interval of follow-up)

Patient	Hemiparesis		Aphasia		Interval
	Pre-op	Follow-up	Pre-op	Follow-up	(days)
Grade III					
1	+	+	+	+	1540
2	−	−	+	±	1273
3	−	+	−	−	532
4	−	−	+	±	470
5	−	−	−	−	1503
6	−	+	−	±	763
Grade IV					
7	−	+	+	+	240
8	−	+	+	+	93
9	−	+	+	+	486
10	−	−	−	−	139
11	−	+	−	−	442
12	+	+	−	−	385
13	−	−	−	+	674

3.6 Detection of change on patients' CSTs and AFs

The CST and the AF are most commonly investigated in studies of tractography because CST is correlated with voluntary motor function and AF is responsible for language function. Detection of changes on patients' CSTs and AFs was performed by comparing

their datasets to corresponding templates of healthy volunteers along the x, y, and z axes. Templates of CST and AF along the x, y, and z axes based on DTI_FA, DTI_MD and DKI_MK were shown in Figure 12. Every template consisted of two curves that represented upper and lower thresholds in corresponding positions along the CST or AF. Templates of CST and AF were different between the left and right.

By comparing patients' datasets to corresponding templates, coordinates were recorded, and change was visualized on tracts as shown in Figure 13. A large portion of the dataset of left AF from patient #7 was under the lower threshold of the left AF template. Coordinates of change were reflected on left AF, and the abnormal portion of left AF was confirmed. Using this method, changes on bilateral CST and AF were confirmed on DTI_FA, DTI_MD, and DKI_MK for all 13 patients.

Patient #1: For the left CST, an increased DTI_MD, and decreased DTI_FA and DKI_MK were found; for the right CST, an increased DTI_MD was found. For the left AF, an increased DTI_MD, and decreased DTI_FA and DKI_MK were found.

Patient #2: For the left CST, increased DTI_FA and DKI_MK were found; for the right CST, an increased DTI_MD and a decreased DTI_FA were found.

Patient #3: For the left CST, an increased DTI_MD was found; for the right CST, an increased DTI_MD was found. For the left AF, an increased DTI_MD, and decreased DTI_FA and DKI_MK were found.

Patient #4: For the left CST, increased DTI_MD and DKI_MK were found; for the right CST, an increased DTI_FA was found.

Patient #5: For the right CST, increased DTI_FA, DTI_MD, and DKI_MK were found. For the left AF, an increased DTI_MD was found; for the right AF, an increased DTI_FA was found.

Patient #6: For the right CST, an increased DKI_MK was found. For the left AF, an increased DTI_MD was found; for the right AF, an increased DTI_MD was found.

Patient #7: For the left CST, changes (increase and decrease) in DTI_MD, and an increased DKI_MK were found; for the right CST, increased DTI_FA and DKI_MK, and

a decreased DTI_MD were found. For the left AF, an increased DTI_MD, and decreased DTI_FA and DKI_MK were found; for the right AF, increased DTI_MD and DKI_MK were found.

Patient #8: For the left CST, an increased DTI_MD, and changes (increase and decrease) in DTI_FA and DKI_MK were found; for the right CST, increased DTI_FA and DKI_MK, and a decreased DTI_MD were found. For the left AF, an increased DTI_MD, and decreased DTI_FA and DKI_MK were found; for the right AF, an increased DKI_MK, and a decreased DTI_MD were found.

Patient #9: For the left CST, increased DTI_MD and DKI_MK were found; for the right CST, a decreased DTI_MD was found. For the left AF, a decreased DTI_MD was found.

Patient #10: For the left CST, an increased DTI_FA was found; for the right CST, changes (increase and decrease) in DKI_MK, and a decreased DTI_MD were found. For the left AF, an increased DTI_MD was found; for the right AF, an increased DTI_MD, and decreased DTI_FA and DKI_MK were found.

Patient #11: For the left CST, increased DTI_MD and DKI_MK were found; for the right CST, an increased DKI_MK was found. For the left AF, an increased DTI_FA was found; for the right AF, an increased DTI_MD and a decreased DKI_MK were found.

Patient #12: For the left CST, increased DTI_MD and DKI_MK were found; for the right CST, an increased DTI_MD, and decreased DTI_FA and DKI_MK were found. For the left AF, an increased DTI_MD was found; for the right AF, an increased DTI_MD and a decreased DKI_MK were found.

Patient #13: For the right CST, an increased DTI_MD and a decreased DKI_MK were found. For the left AF, an increased DTI_MD, and decreased DTI_FA and DKI_MK were found; for the right AF, an increased DTI_MD, and decreased DTI_FA and DKI_MK were found.

3.7 Combinations of change in DTI_FA, DTI_MD, and DKI_MK in relation to hemiparesis or aphasia

Compared to templates derived from healthy volunteers, there were four possible changes: (1) no change, (2) an increased value compared to the corresponding template, (3) a decreased value compared to the corresponding template, and (4) changes with both increased and decreased value compared to the corresponding template. By combining DTI_FA, DTI_MD, and DKI_MK, all 64 possible changes could be analyzed for CST and AF.

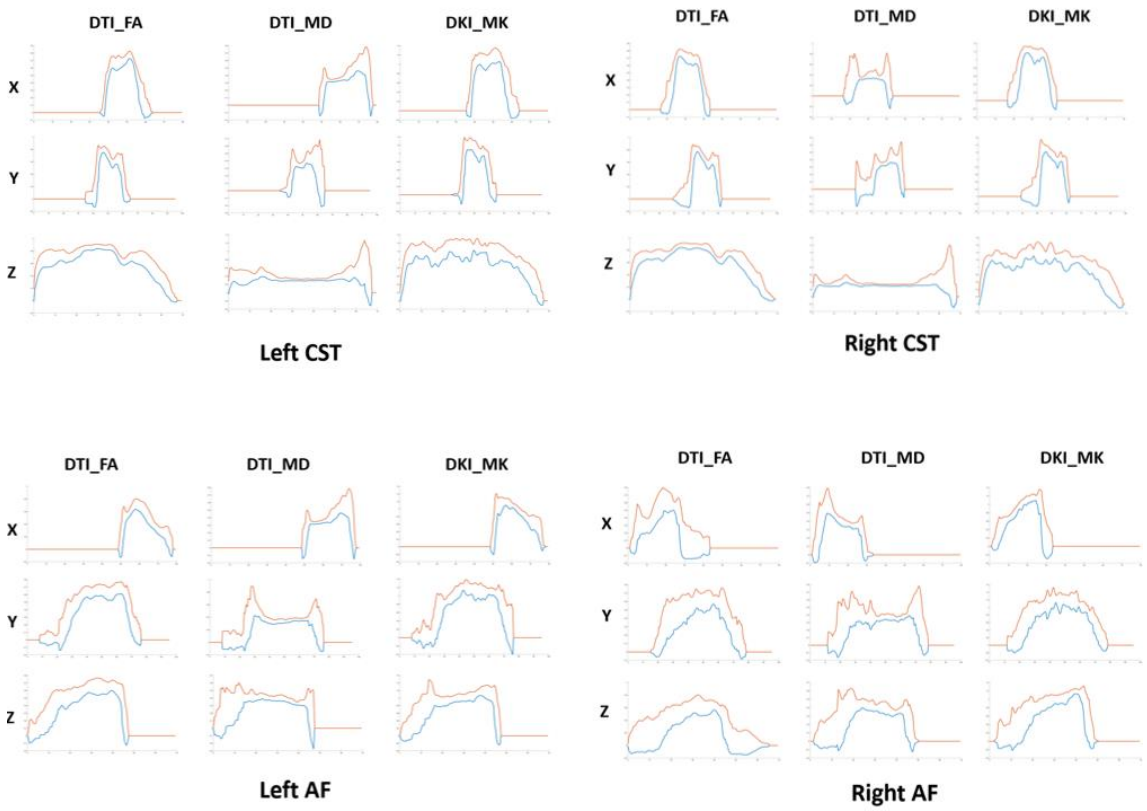

Figure 12. Template of bilateral CST and AF

(red: upper threshold (mean + SD), blue: lower threshold (mean − SD))

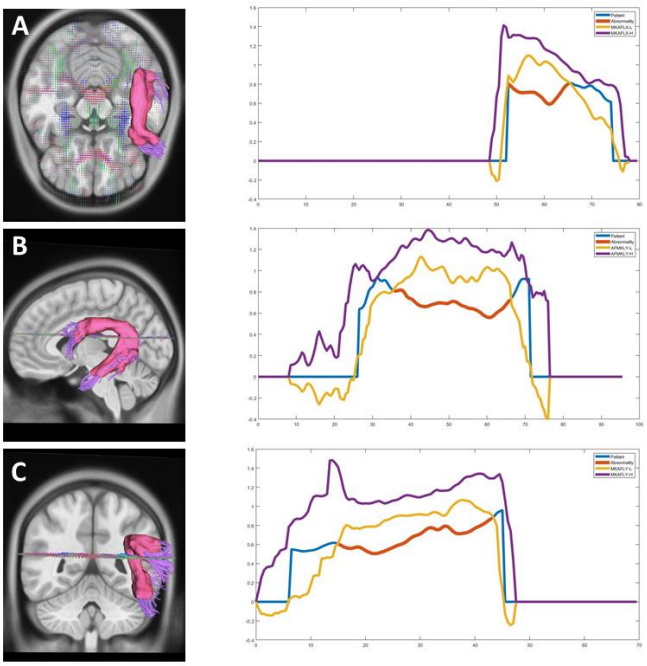

Figure 13. Changes of left AF based on DKI_MK from patient #7

(Datasets shown along x, y, and z axes (Figures A, B, and C, respectively) and their corresponding datasets extracted from fibers compared to templates of healthy volunteers. Data extracted from patient #7 is shown in blue, part of which is highlighted in red. The red portion of the curve was under the lower threshold of the templates, and coordinates were recorded accordingly. On the left, part of the purple fiber tracts were covered in pink, indicating regions of a decreased DKI_MK based on coordinates derived from the templates.)

After comparison with templates, changes were found in CST and AF as listed in Table 6. A total of 13 groups of changes were found in the tracts in relation to hemiparesis or aphasia. These were 9 groups of changes in CST, and 5 in AF. Some groups were common to both tracts. 1) decreased DTI_FA and DKI_MK, and an increased DTI_MD were found; 2) increased DTI_FA and DKI_MK were found; 3) an increased DTI_MD was found; 4) increased DTI_MD and DKI_MK were found; 5) no change was found in parametric maps projected on fiber tracts, and patients' datasets were within the templates' thresholds;

6) an increased DKI_MK was found; 7) changes (increase and decrease) in DTI_MD, and an increased DKI_MK were found; 8) changes (increase and decrease) in DTI_FA and DKI_MK, and an increased DTI_MD were found; 9) a decreased DTI_MD, and changes (increase and decrease) in DKI_MK were found; 10) an increased DTI_MD and a decreased DKI_MK were found; 11) a decreased DKI_MK was found; 12) an increased DTI_FA was found; 13) a decreased DTI_MD and an increased DKI_MK were found.

Table 6. Combinations of changes for CST and AF

CST				AF			
Group	DTI_FA	DTI_MD	DKI_MK	Group	DTI_FA	DTI_MD	DKI_MK
1	↓	↑	↓	1	↓	↑	↓
2	↑	-	↑	2	-	-	-
3	-	↑	-	3	-	↑	-
4	-	↑	↑	4	-	↓	-
5	-	-	-	5	↑	-	-
6	-	-	↑	6	-	↑	↑
7	-	↑+↓	↑	7	-	↓	↑
8	↑+↓	↑	↑+↓	8	-	↑	↓
9	-	↓	↑+↓				
10	-	↑	↓				

As shown in Tables 7 and 8, a decreased DTI_FA was always found concurrent with an increased DTI_MD and a decreased DKI_MK. When changes (increase or decrease) were found in DTI_FA, changes (increase or decrease) were also found in DKI_MK. There was a strong correlation between the FAV and MKV ($r = 0.815$, $p = 0.004$). Correlation between FAV% and MKV% was also significant ($r = 0.794$, $p = 0.006$). No significant correlation was found between the FAV of a decreased DTI_FA and MDV of an increased

DTI_MD (r = 0.619, p = 0.102), but correlation between FAV% of a decreased DTI_FA and MDV% of an increased DTI_MD was found to be significant (r = 0.854, p = 0.007). There was a strong correlation between MDV of an increased DTI_MD and MKV of changes (increase or decrease) in DKI_MK (r = 0.808, p = 0.001). Correlation between MDV% of an increased DTI_MD and MKV% of changes (increase or decrease) in DKI_MK was also significant (r = 0.824, p = 0.001).

Table 7. Volume and percentage of change on CSTs in relation to hemiparesis ('H': higher value than the upper threshold of templates in the corresponding position, 'L': lower value than the lower threshold of templates in the corresponding position; '-': no change was found (i.e. within the range of the templates' thresholds))

	FAV (mm³)		**FAV %**		**MDV (mm³)**		**MDV %**		**MKV (mm³)**		**MKV %**	
	H	L	H	L	H	L	H	L	H	L	H	L
1	-	5392		53.2	4920	-	48.5	-	-	3056		30.1
2	624	-	10.1		-	-	-	-	432	-	7.0	-
3	-	-	-	-	24	-	0.3	-	-	-	-	-
4	-	-	-	-	16	-	0.2	-	48	-	0.5	-
5	-	-	-	-	-	-	-	-	-	-	-	-
6	-	-	-	-	-	-	-	-	32	-	0.3	-
7	-	-	-	-	392	160	5.0	2.0	352		4.5	
8	2376	16	25.3	0.2	2632	-	28.1		408	456	4.4	4.8
9	-	-	-	-	144	-	1.6		480	-	5.4	
10	-	-	-	-	-	608	-	5.9	264	984	2.6	9.5
11	-	-	-	-	-	-	-	-	72	-	0.6	-
12	-	424		5.6	2512	-	33.0	-	-	976	-	12.8
13	-		-		440	-	5.0	-	-	512	-	5.8

Table 8. Volume and percentage of change on left AFs in relation to aphasia ('H': higher value than the upper threshold of templates in the corresponding position, 'L': lower value than the lower threshold of templates in the corresponding position; '-': no change was found (i.e. within the range of the templates' thresholds))

	FAV (mm³)		FAV %		MDV (mm³)		MDV %		MKV (mm³)		MKV %	
	H	L	H	L	H	L	H	L	H	L	H	L
1	-	4824	-	49.7	5656	-	58.3	-	-	3992		41.2
2	-		-		-	-	-	-	-		-	
3	-	1896	-	10.4	11072	-	60.9	-	-	2744		15.1
4	-	-	-		-	-	-	-	-	-	-	-
5	-	-	-		1240	-	11.7	-	-	-	-	-
6	-	-	-		32	-	0.2	-	-	-	-	-
7	-	9176	-	59.7	11152	-	72.6	-	-	9200		59.9
8	-	7704	-	85.1	8296	-	91.6			6656		73.5
9	-	-	-	-	-	248		1.8	-	-	-	-
10	-	-	-	-	4239		27.8	-	-	-	-	-
11	80	-	0.5	-	-		-	-	-	-	-	-
12	-	-	-	-	1576		8.0	-	-	-	-	-
13	-	16	0.1	-	4352		38.2	-	72	-	0.6	-

3.8 Relationship between brain lesion and change of fiber tracts

The spatial relationships between brain lesions (tumor and peritumoral edema) and the change of fiber tracts (shown in Figures 13 and 14) can be divided into three groups: 1) the fiber tract completely or partially covered by lesion, 2) the fiber tract partially 'kissing' lesion, and 3) change in fiber tracts distant from lesion. For the left CST, patients #1, # 3,

#4, #7, and #8 belonged to group 1, and patients #9 and #11 belonged to group 3. For the right CST, patient #12 belonged to group 1, patient # 13 belonged to group 2, and patients #6 and #10 belonged to group 3. For the left AF, patients #1, #4, #7, #8, and #9 belonged to group 1, patient #2 belonged to group 2, and patients #6 and #13 belonged to group 3. For the right AF, patient #13 belonged to group 1, patient #6 belonged to group 2, and patients #1, #2, #4, #7, #8, and #9 belonged to group 3.

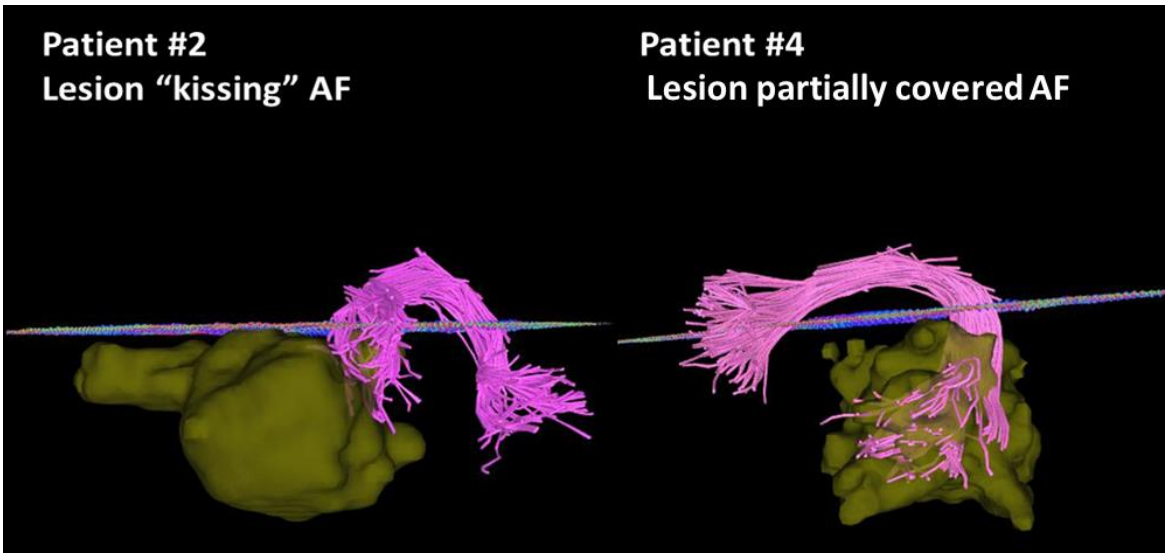

Figure 14. Spatial relationships between brain lesion and AF in patients #2 and #4

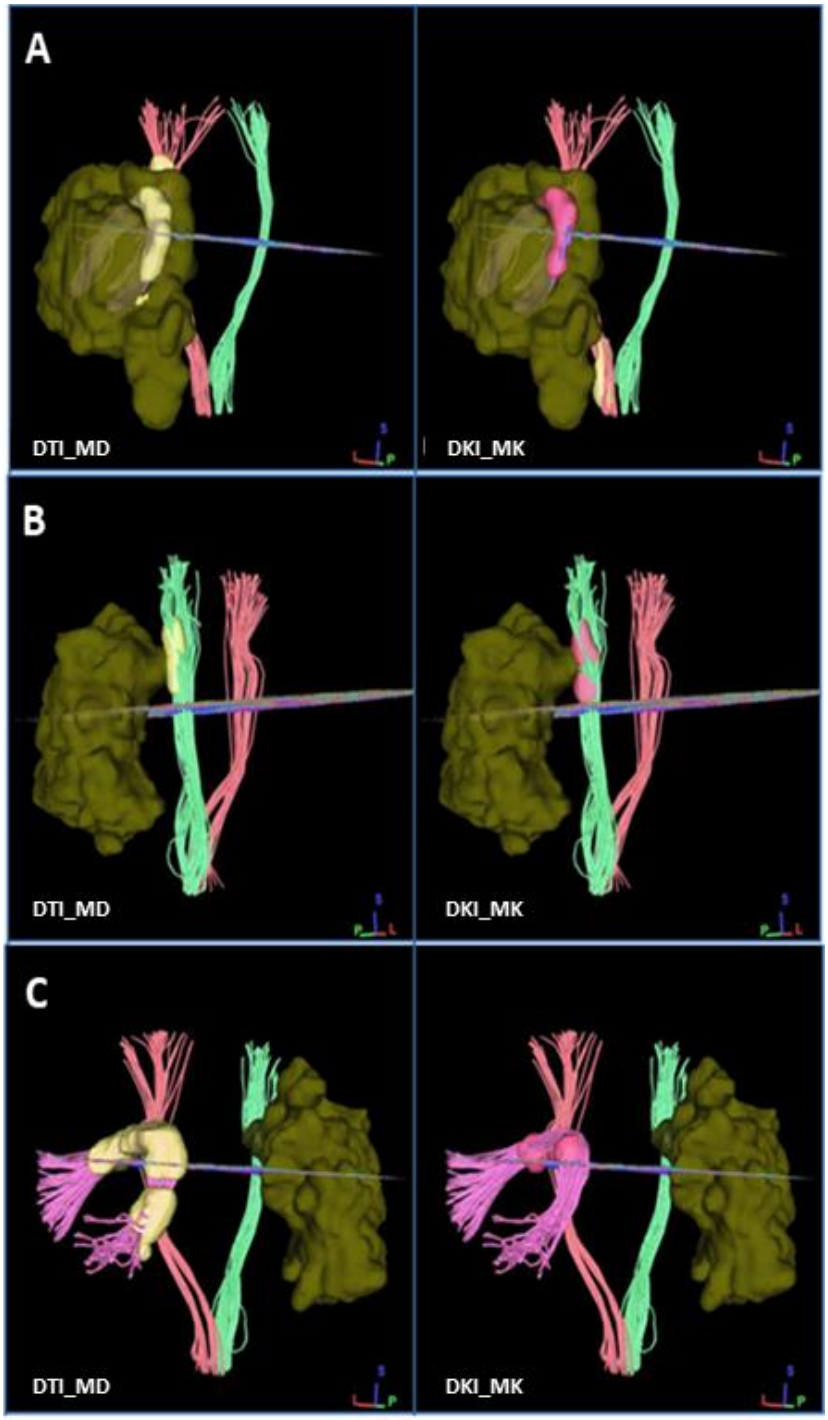

Figure 15. The spatial relationships between brain lesions and changes on dysfunctional fiber tracts

(A: fiber tracts completely or partially covered by lesion, B: part of the fiber tract 'kissing' the boundary of lesion, C: fiber tract distant from the lesion, yellow: an increased value, pink: a decreased value)

3.9 Pattern for indication and prediction of dysfunction in relation to CST and AF

Combining clinical symptoms such as hemiparesis and aphasia of patients and changes found, on both CST and AF, a pattern based on 13 groups of change combinations.

In the left CST, patients who presented with either persisting or emerging right hemiparesis in the follow-up are listed in Table 9. A decreased DTI_FA and an increased DTI_MD concurrent with a decreased DKI_MK were found in two of the three patients who presented with preoperative right hemiparesis (patients #1 and #8); changes (increase and decrease) in DTI_MD, and an increased DKI_MK, were found in the other (patient #7). In all five patients who presented with right hemiparesis in the follow-up, an increased DTI_MD concurrent with changes (increase or decrease) in DKI_MK were found, except for in one (patient #3). Among them, increased DTI_MD and DKI_MK was found in one patient (patients #9) who presented with emerging right hemiparesis.

In the right CST, patients who presented with either persisting or emerging left hemiparesis in the follow-up are listed in Table 10. A decreased DTI_FA and an increased DTI_MD concurrent with a decreased DKI_MK were found in the one patient who presented with preoperative left hemiparesis (patient #12). Left hemiparesis was persisting in this patient. In the follow-up, an increased DTI_MD concurrent with a decreased DKI_MK was found in one of the three patients who presented with left hemiparesis (patients #12). In the other two patients (patient #6 and #11), an increased DTI_MD were found.

Table 9. Change on left CST and right hemiparesis of patients

('+': positive symptom, '−': negative symptom, '±': symptom once appeared but vanished at the end of observation, 'H': an increased value, 'L': a decreased value; '−': no change was found (i.e. within the range of templates' thresholds))

	Relationship between CST and lesion	Hemiparesis		DTI_FA	DTI_MD	DKI_MK
		Pre-op	Follow-up			
1	superior endpoint covered	+	+	L	H	L
3	partially covered	−	+	−	H	−
7	partially covered	+	+	−	H+L	H
8	partially covered	+	+	L+H	H	L+H
9	distant	−	+	−	H	H

Table 10. Change on right CST and left hemiparesis of patients

('+': positive symptom, '−': negative symptom, '±': symptom once appeared but vanished at the end of observation, 'H': an increased value, 'L': a decreased value; '−': no change was found (i.e. within the range of templates' thresholds))

	Relationship between CST and lesion	Hemiparesis		DTI_FA	DTI_MD	DKI_MK
		Pre-op	Follow-up			
6	distant	−	+	−	H	−
11	distant	−	+	−	H	−
12	partially covered	+	+	L	H	L

In the left AF, patients who presented with persisting, emerging, or alleviating aphasia are listed in Table 11. A decreased DTI_FA and an increased DTI_MD concurrent with a decreased DKI_MK were found in three of the six patients with preoperative aphasia (patients #1, #7 and #8). No change was found in two of those seven patients (patients #2 and #4), a decreased DTI_MD in another (patient #9). In the follow-up, a decreased DTI_FA and an increased DTI_MD concurrent with a decreased DKI_MK were found in one patient who presented with emerging aphasia (patient #13). Of the three patients who presented with alleviating aphasia, no change was found in DTI_FA, DTI_MD, or DKI_MK in two (patients #2 and #4); an increased DTI_MD was found in the other patient (patient #6) who presented with emerging aphasia in the follow-up but alleviated and cured at the end of the follow-up.

Table 11. change on left AF and aphasia of patients

('+': positive symptom, '−': negative symptom, '±': symptom once appeared but vanished at the end of observation, 'H': an increased value, 'L': a decreased value; '−': no change was found (i.e. within the range of templates' thresholds))

	Relationship between AF and lesion	**Aphasia**		**DTI_FA**	**DTI_MD**	**DKI_MK**
		Pre-op	Follow-up			
1	both endpoints covered	+	+	L	H	L
2	kissing	+	±	−	−	−
4	posterior endpoint covered	+	±	−	−	−
6	distant	−	±	−	H	−
7	completely covered	+	+	L	H	L
8	both endpoints covered	+	+	L	H	L
9	anterior endpoint covered	+	+	−	L	−
13	distant	−	+	L	H	L

In the right AF, patients who presented with persisting, emerging, or alleviating aphasia are listed in Table 12. A decreased DTI_FA and an increased DTI_MD concurrent with a decreased DKI_MK was found in one patient who presented with emerging aphasia in the follow-up (patient #13) and an increased DTI_MD in another (patient #6). Either an increased DTI_MD (patient #6) or no change in DTI_FA, DTI_MD, or DKI_MK was found in patients who presented with alleviating aphasia (patients #2 and #4).

Table 12. Change on right AF and aphasia of patients

('+': positive symptom, '−': negative symptom, '±': symptom once appeared but vanished at the end of observation, 'H': an increased value, 'L': a decreased value; '−': no change was found (i.e. within the range of templates' thresholds))

	Relationship between AF and lesion	**Aphasia**		**DTI_FA**	**DTI_MD**	**DKI_MK**
		Pre-op	Follow-up			
1	distant	+	+	−	−	−
2	distant	+	±	−	−	−
4	distant	+	±	−	−	−
6	kissing	−	±	−	H	−
7	distant	+	+	−	H	H
8	distant	+	+	−	L	H
9	distant	+	+	−	−	−
13	posterior endpoint covered	−	+	L	H	L

The pattern found in patients with persisting hemiparesis and aphasia, ‘an increased DTI_MD and changes (increase or decrease) in DKI_MK’, summarizes the relationship between changes found on CSTs with hemiparesis and left AFs with aphasia. The relationship between changes found on right AFs and aphasia did not follow this pattern. When relating this pattern to hemiparesis and aphasia in the follow-up, it seemed to present with 75.0% sensitivity and 87.5% specificity.

False negative predictions of aphasia based on the pattern were found in four patients (aphasia in patients #2, #4, #6, and #9, respectively). However, aphasia in three of them (patients #2, #4, and #6) was gradually improved, vanishing by the end of observation. Aphasia was persistent in one patient (patient # 9), and the anterior endpoint of his left AF was found covered in lesions. False negative predictions of hemiparesis were found in three patients (patients #3 and #6), who began to show early signs of hemiparesis by the end of observation, and one of these two died (patient #6); therefore, not enough follow-up information was acquired to explain the hemiparesis that did not match the pattern.

False positive predictions of hemiparesis were found in three patients (patients #3, #12 and #13), and a false positive prediction of aphasia was found in one patient (patient #3). It is worth noting that patient #3, aged 70 years, was the eldest among all recruited patients, and patient #12, aged 66 years, was the second eldest. There was an enormous age discrepancy between these two patients and healthy volunteers. And patient #13 was unable to walk or stand at the end of the follow-up with a KPS (Karnofsky Performance Status) 20%, yet ‘hemiparesis’ is not mentioned.

4 Discussion

Part 1: DKI in Interhemispheric Asymmetry

By using TBSS analysis in DTI- and DKI-based parametric maps, interhemispheric asymmetry was found. Both leftward and rightward asymmetries were found in CST, Fma, ILF, IFOF, SLF, UF, CB, and ATR. Leftward asymmetry was found in Fmi according to DTI_FA, while according to DKI_FA, concurrent leftward and rightward asymmetries were found only in CST. Leftward asymmetry was found in Fmi, CB, and ATR, and rightward asymmetry was found in ILF. According to other maps, such as DTI_MD, DKI_MD, and DKI_MK, fewer significant clusters were found compared to DTI_FA and DKI_FA.

Significant differences were found by directly comparing DTI- and DKI-derived parametric maps. Both fractional anisotropy and mean diffusivity were found to be significantly higher in DKI-derived parametric maps than in DTI-derived parametric maps, both occupying 79.06% of the skeleton. No significant effect was found for handedness or gender.

4.1 Asymmetry of fiber tracts

In our study, either leftward or rightward asymmetry was found in nine major fiber tracts (CST, Fmi, Fma, ILF, IFOF, SLF, CB, and ATR), although DTI- and DKI-based parametric maps differed. Instead of comparing tracts on several chosen levels, such as PLIC of the CST as in many other studies, TBSS analysis has enabled comparison of all image voxels between bilateral tracts. Of note, almost all nine fiber tracts demonstrated both leftward and rightward asymmetries on DTI_FA except Fmi, while the unilateral asymmetry of the fiber tracts was more likely based on DKI_FA. Tracts detected with leftward or rightward asymmetry were fewer on DTI_MD, DKI_MD, and DKI_MK. DTI_FA and DKI_FA seemed to be more sensitive in detecting hemispheric asymmetry than other parametric maps.

The anatomical locations of asymmetry in the brain, based on the DTI_FA map, corresponded to previous studies, especially with regard to the asymmetry observed in the cingulum bundle and other fibers (Buchel et al., 2004; Gong et al., 2005b; Westerhausen et al., 2007; O'Donnell et al., 2009). Leftward asymmetry was found in cingulum bundle in both DTI_FA and DKI_FA, which is similar to previous studies based on DTI (Gong et al., 2005b; Huster et al., 2009; O'Donnell et al., 2009). Most segments of the cingulum were found to be left-dominant except for the posterior part, which was detected by comparing the FA value, which were corresponded with the distributions of asymmetric regions in our findings (Gong et al., 2005b). Leftward asymmetry was also frequently reported in SLF based on DTI studies (Buchel et al., 2004; Powell et al., 2006; Catani et al., 2007), which is consistent with our findings based on DTI_FA. A much larger cluster size was found on leftward asymmetry than rightward asymmetry on SLF based on DTI_FA, but no asymmetry was found on SLF based on DKI_FA. Leftward asymmetry was found in Fmi and Fma (Jahanshad et al., 2010), which is in accordance with findings on DKI_FA, but inconsistent with findings on DTI_FA. Both leftward and rightward asymmetries were found in CST based on DTI_FA and DKI_FA, similar to the findings of previous studies. Some studies have report leftward asymmetry on CST (Westerhausen et al., 2007), while others reported rightward asymmetry at the same level (Imfeld et al., 2009), both using FA value for comparison. These findings indicate that asymmetry in the CST is inconsistent. Both leftward and rightward asymmetries were also reported in IFOF (Rodrigo et al., 2007; Thiebaut de Schotten et al., 2011), ILF (Hasan et al., 2010; Thiebaut de Schotten et al., 2011) and UF (Hasan et al., 2009; Yasmin et al., 2009). Interestingly, these tracts have been found to possibly play a role in neurological disorders such as autism and schizophrenia (Kubicki et al., 2002; Thomas et al., 2011). Rightward asymmetry in ATR was less studied but was reported to correlate with cognitive dysfunction (Mamah et al., 2010).

4.2 Asymmetry and laterality

Interhemispheric asymmetry has been revealed with functional lateralization (Toga and Thompson, 2003). According to previous studies, regions with leftward asymmetries were assumed to correlate with voluntary motor function and language, while regions with rightward asymmetries are mainly related to the function of spatial attention, facial recognition, emotion, and memory (Shu et al., 2015).

A larger cluster was found on regions related to language and auditory processing on the left hemisphere (Steinmetz, 1996; Foundas et al., 1998). Nonetheless, in asymmetry studies based on DTI, a higher FA value was found in the precentral gyrus, which is contralateral to the dominant hand – either statistically significant or shown by a trend corresponding with it – while a higher MD value was observed for the unilateral hemisphere (Buchel et al., 2004; Ardekani et al., 2007; Westerhausen et al., 2007). However, asymmetry not only exists in the cortical and subcortical regions but has also been reported in white matter. Asymmetry in fiber tracts may contribute to a better understanding of functional lateralization.

The CST is one of the most common fiber tracts for studying asymmetry, and it has indeed been found on the CST (Westerhausen et al., 2007; Imfeld et al., 2009; Thiebaut de Schotten et al., 2011). These studies have revealed leftward asymmetry on the CST between hemispheres. Whether the difference in CST (voxels, regional values of parametric maps, or volumes) is directly related to lateralization or dexterity is still not clear. Language function has long been proven to be lateralized by Broca and Wernicke, with which the AF is related (Sreedharan et al., 2015; Silva and Citterio, 2017). Besides, the AF is considered as the fourth part of SLF that connects the frontal and superior temporal gyrus (Makris et al., 2005; Dick and Tremblay, 2012). Similar to our findings in DTI_FA, SLF was also found to be leftward dominant. However, the anterior segment of the AF is rightward lateralized (Buchel et al., 2004; O'Donnell et al., 2009; Thiebaut de Schotten et al., 2011), while the long segment of the AF was frequently reported to be leftward lateralized (Catani et al., 2007; Hasan et al., 2010; Thiebaut de Schotten et al.,

2011), suggesting that asymmetry might be region-dependent and various parts of a fiber tract present heterogeneous asymmetry. ILF in the left dominant brain could have played a role in the language pathway, especially for semantic language processing, but its function could be compensated (Mandonnet et al., 2007). However, ILF was found to be rightward dominant in DTI_FA, DTI_MD, and DKI_FA in our study.

There is still no conclusion as to whether the relationship between asymmetry and laterality is more a phenomenon of grey matter or white matter fibers. Multiples factors like genetics, environmental factors, developmental phase, aging, etc. might also contribute to hemispheric asymmetry.

4.3 Comparison between model-dependent parametric maps

DTI_FA, DTI_MD, DKI_FA, and DKI_MD are all model- and algorithm-dependent parametric maps. As both DTI- and DKI-based parametric maps were derived using the same algorithm, noticeable differences between parametric maps were derived from the differences between the DKI-fitting model and DTI-fitting model. A comparison was done in a voxel-wise manner, and fractional anisotropy was higher in DKI_FA than in DTI_FA, and mean diffusivity was higher in DKI_MD than in DTI_MD, respectively, which was concordant with previous studies applying the same method (Lanzafame et al., 2016). Significant clusters found in the comparison between these maps revealed a significant model-dependent effect.

DTI uses a Gaussian approximation of the probability diffusion function through estimation of the rank-2 diffusion tensor *D*, which allows a directional diffusion profile to be captured by a 3×3 tensor, while DKI is based on non-Gaussian diffusion with an estimation of a rank-4 apparent kurtosis tensor *W* that allows directional kurtosis to be characterized by a 3×3×3×3 tensor matrix (Steven et al., 2014; Lanzafame et al., 2016).

Furthermore, targeted asymmetric regions in DTI_FA were mostly found in the areas where two or more fiber tracts probably cross. The assumption of single fiber orientation in DTI leads to a reduced number of tracts being detected in areas of fiber crossing and

might bias the calculations of structural asymmetry (Lee et al., 2014). This was also proven by a reduced number of asymmetric regions in DTI_MD and DKI_MD, while they are the average of eigenvector (Le Bihan et al., 2001). Many studies have claimed that FA values are considered to reflect the integrity of white matter fibers, axonal density, degree of axonal alignment, myelination, and organization and fiber coherence within a given voxel, and as a result regarded them as an index that reflects structural connectivity and integrity (Angstmann et al., 2016). MD, on the other hand, is a parameter that measures the physicochemical properties of the nervous system (Di Paola et al., 2010). While water diffusion in brain tissue is sensitive to microstructures like myelin sheaths and cell membranes, variability in FA is greatly reduced in areas of single fiber population because much of the variation is caused by crossing fiber tracts, suggesting that FA as a marker for white matter integrity is unprecise – as many studies have claimed (Alexander et al., 2007).

As a result, DTI_FA and DTI_MD based on Gaussian distribution may not be capable of measuring the exact movement of water molecules because the brain's microstructures are not an ideally homogenous liquid for Gaussian distribution (Tuch et al., 2003). And based on the monoexponential model, DTI-based parameters are highly dependent on the selection of b values (Veraart et al., 2011). Neither DTI_FA nor DTI_MD can correctly deal with multiple fibers within one voxel.

As DKI is based on a second-order polynomial model, estimation of diffusion (Veraart et al., 2011) and kurtosis (Jensen and Helpern, 2010) parameters were independent of b values. DKI_MD measuring mean diffusivity in a given voxel based on the DKI model also presents limited capability in detecting crossing fibers, but DKI_FA measuring directional anisotropy is capable of resolving coherent fibers within one voxel (Zhu et al., 2015). DKI_MK characterizes the mean deviation from Gaussian distribution, providing relatively more accurate information in brain tissue (Jensen and Helpern, 2010), especially in regions with crossing fibers (Lazar et al., 2008), which makes it useful for evaluating complex brain microstructures (Jensen et al., 2005a; Lazar et al., 2008).

Significant clusters found in DTI-based parametric maps might not fully characterize asymmetric fiber tracts. In order to access the advantages of DKI, both DTI-fitting and DKI-fitting methods should be applied to DWI data separately. Even though DKI is an extension of DTI, and they can both be structured into a linear regression form based on the natural logarithm of diffusion-weighted MR signals (Veraart et al., 2013). DTI-based parametric maps such as DTI_FA and DTI_MD were not equivalent to DKI_FA and DKI_MD theoretically, because estimations of these diffusion parameters were based on different models, and our direct comparison also demonstrated the model-dependent discrepancy between DTI- and DKI-based diffusion parameters.

4.4 Handedness and gender related to interhemispheric asymmetry

Consistent with our findings, gender was found to have little effect on interhemispheric asymmetry in many other studies (Gong et al., 2005b; Westerhausen et al., 2007; Huster et al., 2009; Lebel and Beaulieu, 2009; Hasan et al., 2010; Takao et al., 2011). In another study, a gender-by-hemisphere effect was shown significant only on ILF in children and adolescents (Hasan et al., 2010). It is noteworthy that neither handedness was found to affect interhemispheric asymmetry. Previous studies have revealed that no significant correlation was found between the asymmetry of the CST at the level of internal capsule and handedness (Westerhausen et al., 2007). Regions where right-handed people were reported to have higher values than the contralateral side were found to be statistically significant by comparing FA values in various levels of the CST based on diffusion tensor tractography (Westerhausen et al., 2007; Seizeur et al., 2014), but not necessarily correlated with dexterity (Westerhausen et al., 2007). On the contrary, voxel-based morphometry (VBM) of T1-weighed images has revealed a significant relationship between interhemispheric asymmetry and handedness (Good et al., 2001), and other macrostructural studies have also shown signs, like a deeper central sulcus in the dominant hemisphere (Amunts et al., 2000) or a more dorsal shape of the human hand

knob in the left hemisphere of right-handed people as compared to left-handed people (Sun et al., 2012). However, in another study, no handedness-related asymmetry was reported in the bilateral primary motor cortex (Ciccarelli et al., 2003).

The relationship between asymmetry in the fiber tract and lateralization is still not fully understood. On the one hand, asymmetry differs in various parts of the fiber tract. On the other hand, asymmetry in the fiber tracts does not necessarily equal anatomical asymmetry in the human brain. Besides, the possibility that asymmetry in a functional cortex rather than the fiber tract might be decisive in lateralization should also be taken into consideration for understanding asymmetry in the fiber tracts more deeply.

Part 2: DKI in glioma patients

In this part of the study, a new application of DKI has been revealed by detecting changes of the CST and AF that might correlate with prognosis in relation to neurological deficits in high-grade glioma patients. To achieve this, templates of CSTs and AFs derived from healthy volunteers were successfully created, which allowed changes of the tracts to be visualized. Changes could occur on CSTs and AFs that were encased by the tumor, kissing the tumor, or distant from the tumor. Changes on tracts were quantified, and strong correlations were found between DTI- and DKI-based parameters. This indicated changes relating to hemiparesis and aphasia were consistent on both DTI and DKI parametric maps. These findings support our hypothesis that change on the CST and AF might be potentially predictive of outcomes of motor and language deficit with 75% sensitivity and 87.5% specificity. It seemed that the pattern of an increased DTI_MD and changes (increase or decrease) in DKI_MK was concurrent in CST or AF, indicating that fiber tracts were severely affected either by infiltration, edema, or Wallerian degradation.

4.5 Infiltration of glioma as the main cause

One theory about the infiltration of glioma is that tumor cells migrate along fiber tracts (Scherer, 1940). Based on this theory, previous studies have shown that DTI-related

parameters were capable of assessing the extent of the infiltrated area on the CST (Bello et al., 2008; Gao et al., 2017). Significantly higher MD and lower FA were found to indicate infiltration caused by tumor growth as opposed to edema compared to contralateral CST (Delgado et al., 2016). In accordance with our findings, decreased FA was also reported in white matter proximal to high-grade gliomas (Field et al., 2004; Price et al., 2004), which could be explained by Wallerian degradation (Thomalla et al., 2004). Between high- and low-grade glioma, FA was found to be higher and MD was lower in high-grade glioma (Inoue et al., 2005). Both FA and MK were significantly lower in perilesional white matter and tumor centers than that of contralateral normal-appearing white matter (NAWM), not only in grade II and grade III gliomas (Delgado et al., 2017) but also in grade IV glioblastoma, as reported by other studies (Van Cauter et al., 2012; Qi et al., 2017).

An increased MK is related to higher malignancy (Raab et al., 2010) because of higher tumor cellularity, higher heterogeneity, and higher microstructural complexity (Van Cauter et al., 2012; Jiang et al., 2015; Bai et al., 2016), while a low kurtosis found in peritumoral regions suggested a microstructural rearrangement due to tumor infiltration (Delgado et al., 2017). It is noteworthy that all of the comparisons mentioned in previous studies were made between targeted lesions and contralateral white matter, assuming that the contralateral side was ‘normal’. Increased MD and FA in CST have been correlated with postoperative motor dysfunction (Rosenstock et al., 2017). Damage to AF could be predictive of persisting language dysfunction in high-grade glioma patients, to which the percentage of affected fiber tracts is of great importance (Caverzasi et al., 2016).

4.6 Peritumoral edema as a complementary contributor

Either an increased or a decreased DKI_MK was found in regions on fiber tracts in relation to dysfunction in this study. Peritumoral edema might indeed be one of the contributors to the change detected on fiber tracts. MK showed a higher value in peritumoral edema in patients with high-grade glioma than with low-grade glioma (Tan

et al., 2016) because high-grade glioma is characterized by more of a diffusion barrier and a higher microstructural complexity (Kleihues et al., 1995). But overlap in the range of MK values has also been reported in healthy brains compared to brains harboring glioma (Latt et al., 2013).

Besides, there is a possibility that DTI parameters might be normal even in cytotoxic edema when the blood–brain barrier remains intact (Ho et al., 2012). Both FA and MD could be altered by vasogenic edema. A decreased FA and an increased MD were observed compared to contralateral normal-appearing white matter (Holly et al., 2017). A common assumption for this phenomenon is increased extracellular water accumulation due to breakdown of the blood–brain barrier (Lu et al., 2003; Ho et al., 2012). On the other hand, no significant difference was observed in FA and MD of a peritumoral edema area between high- and low-grade glioma (Jiang et al., 2017).

4.7 Timeframe of occurrence

Mean kurtosis was found to be distinctively decreased with age, which might indicate degenerative changes (Falangola et al., 2008; Van Cauter et al., 2012), which allows early detection of Parkinson's disease and differentiates patients of early and advanced stages, which FA and MD failed to reveal (Guan et al., 2019). In an animal model of transient focal ischemia, MK was capable of detecting hyper-acute and acute stroke and showed consistent results, while MD based on DTI tended to change dramatically with time or reperfusion (Cheung et al., 2012; Hui et al., 2012).

Our findings revealed that decreased DTI_FA and DKI_MK concurrent with an increased DTI_MD tended to correlate with long-lasting preoperative motor and language deficits that were prone to persist even after treatment (surgery, radiotherapy, and chemotherapy). In addition, an increased DTI_MD concurrent with changes (either increase or decrease) in DKI_MK were proven to correlate with emerging hemiparesis or aphasia. Whether there is also such a timeframe in the occurrence of DKI_MK, DTI_MD and DTI_FA in fiber tracts infiltrated by glioma, as it is shown in neurodegenerative disease or ischemia,

is still unknown.

4.8 Correlation between DTI- and DKI-based parameters and clinical findings

The pattern of an increased DTI_MD with changes (increase or decrease) in DKI_MK may be caused by a reduction of axonal number or density, infiltration of tumor cells, or degradation of individual fibers, but further study is required. This is because fiber reconstruction was mostly performed by using known anatomical landmarks to seed regions or ROIs (Clark et al., 2003; Yamada et al., 2003; Morita et al., 2011), either manually (Wakana et al., 2004; Wakana et al., 2007) or automatically (Yendiki et al., 2011; Yeatman et al., 2012). The choice for the placement of ROIs might result in variability of fiber reconstruction (Wakana et al., 2007) with utilization of different tracking methods, and the number and volume of fiber changes. Fiber tracts involved in tumor or edema tend to be misdirected because misleading eigenvectors may inaccurately present the orientation of axonal bundles (Berman et al., 2004). It is uncertain from mere visual assessment whether the reconstructed fiber tract is still intact or already disrupted by tumor. This approach provided a possibility for quantitative assessment by comparing fiber tracts of patients to templates derived from healthy volunteers in which slices occupied by fiber tracts were depicted along the x, y, and z axes. When compared to templates, tested fiber tracts exceeding the boundary were found to be displaced. In this way, the detection of tract displacement, as well as direct comparison in corresponding spatial location, were enabled. This method avoids the ambiguity caused by averaging parameters along tracts that are not equally distributed, as previous research suggested that FA varied substantially within a tract (Yeatman et al., 2012). Besides, not every individual tract of a specific trajectory is the same length, and lower FA is unavoidable at crossing fibers, assuming there can only be one single fiber population (Alexander et al., 2007).

Thus, affected white matter fiber tracts were more directly demonstrated in this method

than the commonly used morphological T1 contrast-enhanced fluid-attenuated inversion recovery (FLAIR) and T2-weighted images, thereby this method is capable of predicting vital functions of fiber tracts more accurately. The pattern revealed that regions with an increased DTI_MD and changes (increase or decrease) in DKI_MK could be a result of a combination of various factors such as infiltration, vasogenic edema, Wallerian degradation, and age. Change detected on the CST or AF in accordance with the revealed pattern tended to correlate with persisting hemiparesis or aphasia, while change mismatched with this pattern was found to be potentially connected to a better chance of recovering, especially in grade III glioma patients. Change (either increase or decrease) in DKI_MK, along with an increased DTI_MD was likely to be connected with infiltrated fiber tracts. Change found on the CST or AF distant from tumor might be explained by Wallerian degradation (Thomalla et al., 2004). Based on this method, the overall impact of the tumor was considered instead of focusing on specific parts of the tumor such as the tumor center or peritumoral edema.

Part 3: Interpretation of DTI- and DKI-based parameters

Considerable attention has been given to the application of DKI in recent years due to its feasibility in clinical use. In our study, satisfying results have been revealed by the performance of DKI compared to DTI. Both DKI and DTI were employed in healthy volunteers for detecting interhemispheric asymmetry, as well as in high-grade glioma patients for detecting changes of the CST and AF. As a result, the descriptive and discriminative potential of DTI- and DKI-based parameters were sufficiently explored.

On the one hand, the hindrance of water molecules' movement is due to small compartments like organelles and membranes in the brain's microstructures. With b < 1000 s/mm^2, these small compartments are difficult to detect in DTI. Under this circumstance, the diffusion of water molecules deviates from Gaussian diffusion. However, in DKI with an additional b 2000 s/mm^2, recognition of these small compartments becomes possible. DKI, as a three-dimensional generalization of the

second-order cumulant expansion proposed by Jensen (Jensen et al., 2005a), can indeed be used to reveal both Gaussian and non-Gaussian distribution. Therefore, higher sensitivity to microstructural changes is inherited in the DKI model. Furthermore, DKI is capable of resolving two and three intersecting fibers within one voxel (Lazar et al., 2008). On the other hand, the DKI model is dependent on 21 parameters compared to DTI's six, so high variability is expected to occur in DKI when a short imaging protocol is applied. Variability has also been reported to differ in brain regions, which can lead to a lack of significance (Steven et al., 2014).

MD and FA are the most commonly used DTI-based parameters. MD is calculated by the mean of three eigenvectors and regarded as a molecular diffusion rate, whereas FA is measured by a normalized method of fraction of tensor's magnitude and considered as the directional preference of diffusion (Soares et al., 2013). Basically, MD increases in areas with increased free diffusion, while FA decreases in areas with loss of coherence against the main preferred diffusion orientation. An increased MD and a decreased FA suggested that fiber integrity was damaged or impaired since an increased MD is related to increased diffusion, and a decreased FA is related to loss of coherence (Soares et al., 2013). However, increased FA does not necessarily translate to an intactness of fiber tracts, because increased FA values were reported to correlate with poor outcomes in Williams syndrome (Hoeft et al., 2007).

The most commonly used DKI-based parameter is MK. As the average of deviation from Gaussian diffusion, MK is proportional to the heterogeneity and complexity of brain tissue. Generally, an increased MK is correlated with higher cellularity and microstructural complexity, while a decreased MK indicates a loss of cellular structure (Steven et al., 2014). In other studies, an increased MK could also be interpreted as increased glial activity or severe astrogliosis in brain trauma study (Zhuo et al., 2015), or it served as a biomarker for discriminating high- and low-grade glioma. Additionally, a decreased MK has also been found to correlate with neurodegenerative diseases like Parkinson's (Wang et al., 2011) and Alzheimer's (Falangola et al., 2013), in which a

decreased MK was interpreted as loss of neuron cell bodies, synapses, and dendrites.

That higher fractional anisotropy was found in corresponding voxels in DKI_FA than in DTI_FA can be explained by the finding that crossing fibers are more problematic for FA than for MD (Tournier et al., 2011).

Thus, FA, MD, and MK are scalar maps estimated from mathematical models that cannot directly show pathological or physiological processes. The interpretation of FA, MD, and MK should be done with caution. Firstly, structural differences exist in the different anatomical levels of fiber tracts. Differences in various anatomical locations of the CST were already detected by higher anisotropy in the cerebral peduncle and lower anisotropy in the pons and medulla, to which a highly ordered arrangement of fiber was decisive in a healthy human brain (Virta et al., 1999). With structural complexity, subdivision of the cingulum was achieved by DTI, and little overlap was detected between them (Jones et al., 2013). Different segments of the AF also differed from each other in asymmetry (Buchel et al., 2004; Catani et al., 2007; O'Donnell et al., 2009; Hasan et al., 2010; Thiebaut de Schotten et al., 2011). Secondly, not only tract volume and tract length, but also DTI-based parameters were affected by different tract delineation methods (Sydnor et al., 2018). Thirdly, various factors such as demyelination, inflammation, axonal loss, and gliosis are influences in the white matter fiber tracts that compete against each other. It might be an exaggeration to suggest that increased or decreased measurements certainly mean the brain tissue is going through only one process, ignoring that it may actually the result of a combination of multiple process. Because of the variability presented by both DTI- and DKI-based parameters, higher and lower values can correlate with disease or physiological changes, or even both.

With additional microstructural information adding to DTI, DKI has proved its feasibility in both healthy volunteers and high-grade glioma patients. But the interpretation of DKI characterization has not yet been fully explored. More studies are needed in order to deepen the understanding of DKI and expand its advanced application in clinical practice.

4.9 Limitations

This study, however, is not without limitations. Firstly, the number of healthy volunteers and patients who participated in this study was sufficient, but certainly not large. Secondly, there was a moderate age discrepancy between healthy volunteers and high-grade glioma patients. As age does play a role in changes in white matter, using templates based on younger healthy volunteers might lead to changes detected on patients' CSTs or AFs that were caused by physiological changes. This might explain why some lesions on tracts were detected contralaterally to the tumors but caused no motor or language deficits. Thirdly, the same reconstruction method was applied to DTI and DKI data. Although the application of the reconstruction method to DTI data has been proven to be both practical and feasible, it was not designed specifically for DKI. Different reconstruction protocols should be applied to exploit diffusion kurtosis tractography, such as isolating various tracts from whole-brain tractography yielded by seeding from a particular anatomical position.

4.10 Future Work

As an extension of this study, more right-handed healthy subjects will be recruited in different age groups to minimize the potential influence of age when comparing to templates. Additionally, patients with low-grade glioma will be included in order to test the usefulness of the pattern revealed by DKI for low-grade glioma. For further investigation, follow-up DWI data of patients will be carefully examined in order to see whether the pattern found in our study is connected with persisting or transient symptoms that could be alleviated or healed, and whether there is a time frame between the occurrence of change in DTI_MD and DKI_MK and then DTI_FA. Automatic reconstruction of fiber tracts in both volunteers and patients will also be applied to lessen the possible error caused by manual reconstruction.

To the best of our knowledge, this study is the first to apply DKI on interhemispheric asymmetry based on TBSS analysis. Data has been extracted from CST and AF along three-dimensional directions instead of along tracts to avoid ambiguity. The predictive value of DKI was therefore exploited for the outcome of hemiparesis and aphasia in high-grade glioma patients. Differences and correlation between DTI- and DKI-based parameters have been revealed. In conclusion, application of DKI deepens the understanding of white matter under physiological as well as pathological conditions.

5 Summary

Diffusion tensor imaging (DTI) has become a standard procedure in clinical routine as well as research as it enables the reconstruction and visualization of fiber tracts in the human brain. Due to the simplified assumption the tensor model – a Gaussian distribution of the diffusion – it typically fails to provide neither accurate spatial mapping nor quantification of crossing or kissing fibers. A clinically feasible development might be diffusion kurtosis imaging (DKI), an extension of DTI also integrating non-Gaussian distribution diffusion processes and thereby shall overcome some of its limitations.

The potential DKI will be evaluated in case of the detection of the interhemispheric asymmetry of the white matter in healthy volunteers (n = 20), as well as the analysis of tumor-related impairments of fiber tracts and their correlation with neurological deficits in patients (n = 13) diagnosed with glioma.

In order to analyze interhemispheric asymmetry across the whole brain, especially of nine large fiber tracts, tract-based spatial statistics (TBSS) analysis was performed using DTI- and DKI-based parameters, a laterality index was calculated for asymmetries and DTI- and DKI-based results were compared.

With regard to fractional anisotropy as marker of integrity, asymmetry was found for all nine fiber tracts based on DTI and seven tracts based on DKI. For mean diffusivity, asymmetries were found for three (DTI) and two (DKI) fiber tracts. Regarding mean kurtosis, asymmetry was found in one tract. The interhemispheric asymmetry thereby varied in anatomical location as well as in cluster size. Only small parts of the tracts were affected. A comparison of DTI and DKI showed significantly higher fractional anisotropy and mean diffusivity based on DKI compared to DTI. Gender and handedness did not seem to have any influence.

For the assessment of tumor-related changes of fiber tracts in patients diagnosed with glioma, especially in relation to pre-existing and postoperative neurological deficits (hemiparesis, aphasia), templates for the corticospinal tract and the arcuate fasciculus were created based on DTI- and DKI-derived parameters, respectively. The corticospinal

tract and the arcuate fasciculus were reconstructed for each patient and the associated parametric maps were projected onto the templates. Based on this, alterations along the tracts could be identified and quantified. Alterations were found on fiber tracts regardless of the spatial proximity to the lesion. There was a correlation between alterations based on fractional anisotropy, mean diffusivity and mean kurtosis. Increased mean diffusivity was associated with alteration in mean kurtosis, a decreased fractional anisotropy was found concurrent with a likewise decreased mean kurtosis. In the case of pre-existing neurological deficits (hemiparesis, aphasia) with regard to the changes along the fiber tracts (corticospinal tract, left arcuate fasciculus), most often increased mean diffusivity and altered mean kurtosis was found. Applying this pattern for prediction of corresponding postoperative neurological deficits a sensitivity of 75.0% and a specificity of 87.5% was achieved.

DKI seems to more precisely estimated and depict the underlying microstructure in comparison to DTI. Thereby, in pathological cases especially the mean kurtosis seems to be of special interest. A combination of DTI- and DKI based parameters, particularly with regard to its clinical usability and value, offers great potential in clinical routine.

6 Zusammenfassung

Die Diffusions-Tensor-Bildgebung (DTI) zur Rekonstruktion und Visualisierung von Fasertrakten im Gehirn zählt mittlerweile zu den Standardverfahren in der klinischen Routine und der neurowissenschaftlichen Forschung. Aufgrund der vereinfachenden Annahme des zugrundliegenden Tensormodells - einer Gaußschen Verteilung der Diffusion - ist eine räumlich genaue Abbildung und Quantifizierung z.B. sich kreuzender oder tangierender Faserbahnen nicht gegeben. Eine klinisch praktikable Weiterentwicklung stellt die Diffusions-Kurtosis-Bildgebung (DKI) dar, die das DTI Modell um die Modellierung der nicht-Gaußschen Verteilung der Diffusion erweitert und so den Limitationen entgegen wirken soll.

Das Potential dieser erweiterten Modellierung soll hier nun in Bezug auf die Detektion der interhemispärischen Asymmetrie der weißen Substanz gesunder Probanden (n = 20) evaluiert werden, sowie zur Analyse tumorbedingter Veränderungen von Faserbahnen bei Patienten (n = 13) mit Gliomen und deren Zusammenhang mit neurologischen Defiziten herangezogen werden.

Zur Analyse der Interhemispähren-Asymmetrie wurde sowohl mittels DTI- als auch DKI-basierten Parametern eine Fasertrakt-basierte Analyse der weißen Substanz, insbesondere von neun großen Fasertrakten durchgeführt, bei Asymmetrien ein Lateralitätsindex bestimmt, sowie DTI- und DKI-basierte Ergebnisse verglichen.

Bezüglich der fraktionellen Anisotropie als Marker für die Integrität von Faserbahnen zeigten sich für DTI für alle, basierend auf DKI nur für sieben der neun Trakte Asymmetrien. Für die mittlere Diffusivität fanden sich Asymmetrien für drei (DTI) bzw. zwei (DKI) komplementäre Trakte, für die mittlere Kurtosis nur für einen Trakt. Die interhemisphärische Asymmetrie variierte dabei insgesamt bzgl. der anatomischen Lokalisation als auch in ihrer Ausprägung, nur geringe Anteile der Trakte waren betroffen. Im direkten Vergleich der beiden Modelle zeigte sich eine signifikant höhere fraktionelle Anisotropie und mittlere Diffusivität basierend auf DKI im Vergleich zu DTI. Geschlecht und Händigkeit schienen keinen Einfluss zu nehmen.

Für die Beurteilung tumorassoziierter Veränderungen in den Faserbahnen bei Patienten mit Gliomen insbesondere in Relation zu vorbestehenden und postoperativen neurologischen motorischen und sprachassoziierten Defiziten wurden auf Basis der DTI- und DKI-basierten Parameterkarten Referenzkarten für die Pyramidenbahn sowie den Fasciculus arcuatus erstellt. Für jeden Patienten wurden im Anschluss die Pyramidenbahn und der Fasciculus arcuatus rekonstruiert und die zugehörigen Parameterkarten auf die Schablonen projiziert. Anhand derer konnten für die Patienten Veränderungen entlang der Trakte identifiziert und quantifiziert werden.

Bei Patienten traten dabei im Vergleich zu Gesundprobanden Veränderungen der Diffusionparameter entlang der Trakte auf, egal ob distant oder nähe der Läsion. Es zeigte sich eine Korrelation zwischen der räumlichen Ausdehnung der Veränderungen für die fraktionelle Anisotropie und die mittlere Kurtosis. Eine gesteigerte mittlere Diffusivität stand im Zusammenhang mit einer Veränderung der mittleren Kurtosis, eine verringerte fraktionelle Anisotropie zeigte sich korrelierend zu einer ebenfalls verringerten mittleren Kurtosis. Bei vorbestehenden neurologischen Defiziten (Hemiparese, Aphasie) fand sich in Bezug auf die Veränderungen entlang der Fasertrakte (Pyramidenbahn, Fasciculus arcuatus links) vornehmlich eine gesteigerte mittlere Diffusivtät sowie eine Veränderung der mittleren Kurtosis im Vergleich zum Referenzmodell. Die Anwendung dieser Relation ließ dabei die Vorhersage entsprechender postoperativer neurologischer Defizite mit einer Sensitivität von 75,0 % und einer Spezifität von 87,5 % im Rahmen des Patientenkollektivs zu.

DKI scheint gegenüber dem vereinfachten Modell der DTI eine zum Teil spezifischere Abbildung der zugrundliegenden Mikrostruktur zu ermöglichen. Gerade die mittlere Kurtosis erscheint bei pathologischen Veränderungen dabei eine besondere Rolle zu spielen, so dass die Kombination von DTI- und DKI-basierten Informationen, insbesondere unter dem Aspekt der klinischen Umsetzbarkeit und Nutzbarkeit, Potential für die klinische Routine bietet.

References and Bibliography

Agcaoglu, O., Miller, R., Mayer, A.R., Hugdahl, K., and Calhoun, V.D. (2015). Lateralization of resting state networks and relationship to age and gender. *Neuroimage* 104**,** 310-325. doi: 10.1016/j.neuroimage.2014.09.001.

Alexander, A.L., Lee, J.E., Lazar, M., and Field, A.S. (2007). Diffusion tensor imaging of the brain. *Neurotherapeutics* 4(3)**,** 316-329. doi: 10.1016/j.nurt.2007.05.011.

Amunts, K., Jancke, L., Mohlberg, H., Steinmetz, H., and Zilles, K. (2000). Interhemispheric asymmetry of the human motor cortex related to handedness and gender. *Neuropsychologia* 38(3)**,** 304-312. doi: 10.1016/s0028-3932(99)00075-5.

Angstmann, S., Madsen, K.S., Skimminge, A., Jernigan, T.L., Baare, W.F., and Siebner, H.R. (2016). Microstructural asymmetry of the corticospinal tracts predicts right-left differences in circle drawing skill in right-handed adolescents. *Brain Struct Funct* 221(9)**,** 4475-4489. doi: 10.1007/s00429-015-1178-5.

Arac, N., Sagduyu, A., Binai, S., and Ertekin, C. (1994). Prognostic value of transcranial magnetic stimulation in acute stroke. *Stroke* 25(11)**,** 2183-2186. doi: 10.1161/01.str.25.11.2183.

Ardekani, S., Kumar, A., Bartzokis, G., and Sinha, U. (2007). Exploratory voxel-based analysis of diffusion indices and hemispheric asymmetry in normal aging. *Magn Reson Imaging* 25(2)**,** 154-167. doi: 10.1016/j.mri.2006.09.045.

Bai, Y., Lin, Y., Tian, J., Shi, D., Cheng, J., Haacke, E.M., et al. (2016). Grading of Gliomas by Using Monoexponential, Biexponential, and Stretched Exponential Diffusion-weighted MR Imaging and Diffusion Kurtosis MR Imaging. *Radiology* 278(2)**,** 496-504. doi: 10.1148/radiol.2015142173.

Barrick, T.R., Lawes, I.N., Mackay, C.E., and Clark, C.A. (2007). White matter pathway asymmetry underlies functional lateralization. *Cereb Cortex* 17(3)**,** 591-598. doi: 10.1093/cercor/bhk004.

Basser, P.J., Mattiello, J., and LeBihan, D. (1994a). Estimation of the effective self-diffusion tensor from the NMR spin echo. *J Magn Reson B* 103(3)**,** 247-254. doi:

10.1006/jmrb.1994.1037.

Basser, P.J., Mattiello, J., and LeBihan, D. (1994b). MR diffusion tensor spectroscopy and imaging. *Biophys J* 66(1)**,** 259-267. doi: 10.1016/S0006-3495(94)80775-1.

Beaton, A.A. (1997). The relation of planum temporale asymmetry and morphology of the corpus callosum to handedness, gender, and dyslexia: a review of the evidence. *Brain Lang* 60(2)**,** 255-322. doi: 10.1006/brln.1997.1825.

Behrens, T.E., Berg, H.J., Jbabdi, S., Rushworth, M.F., and Woolrich, M.W. (2007). Probabilistic diffusion tractography with multiple fibre orientations: What can we gain? *Neuroimage* 34(1)**,** 144-155. doi: 10.1016/j.neuroimage.2006.09.018.

Bello, L., Gambini, A., Castellano, A., Carrabba, G., Acerbi, F., Fava, E., et al. (2008). Motor and language DTI Fiber Tracking combined with intraoperative subcortical mapping for surgical removal of gliomas. *Neuroimage* 39(1)**,** 369-382. doi: 10.1016/j.neuroimage.2007.08.031.

Berman, J.I., Berger, M.S., Mukherjee, P., and Henry, R.G. (2004). Diffusion-tensor imaging-guided tracking of fibers of the pyramidal tract combined with intraoperative cortical stimulation mapping in patients with gliomas. *J Neurosurg* 101(1)**,** 66-72. doi: 10.3171/jns.2004.101.1.0066.

Bethmann, A., Tempelmann, C., De Bleser, R., Scheich, H., and Brechmann, A. (2007). Determining language laterality by fMRI and dichotic listening. *Brain Res* 1133(1)**,** 145-157. doi: 10.1016/j.brainres.2006.11.057.

Binder, J.R., Swanson, S.J., Hammeke, T.A., Morris, G.L., Mueller, W.M., Fischer, M., et al. (1996). Determination of language dominance using functional MRI: a comparison with the Wada test. *Neurology* 46(4)**,** 978-984. doi: 10.1212/wnl.46.4.978.

Buchel, C., Raedler, T., Sommer, M., Sach, M., Weiller, C., and Koch, M.A. (2004). White matter asymmetry in the human brain: a diffusion tensor MRI study. *Cereb Cortex* 14(9)**,** 945-951. doi: 10.1093/cercor/bhh055.

Cao, Y., Whalen, S., Huang, J., Berger, K.L., and DeLano, M.C. (2003). Asymmetry of

subinsular anisotropy by in vivo diffusion tensor imaging. *Hum Brain Mapp* 20(2)**,** 82-90. doi: 10.1002/hbm.10130.

Catani, M., Allin, M.P., Husain, M., Pugliese, L., Mesulam, M.M., Murray, R.M., et al. (2007). Symmetries in human brain language pathways correlate with verbal recall. *Proc Natl Acad Sci U S A* 104(43)**,** 17163-17168. doi: 10.1073/pnas.0702116104.

Catano, A., Houa, M., Caroyer, J.M., Ducarne, H., and Noel, P. (1996). Magnetic transcranial stimulation in acute stroke: early excitation threshold and functional prognosis. *Electroencephalogr Clin Neurophysiol* 101(3)**,** 233-239. doi: 10.1016/0924-980x(96)95656-8.

Caverzasi, E., Hervey-Jumper, S.L., Jordan, K.M., Lobach, I.V., Li, J., Panara, V., et al. (2016). Identifying preoperative language tracts and predicting postoperative functional recovery using HARDI q-ball fiber tractography in patients with gliomas. *J Neurosurg* 125(1)**,** 33-45. doi: 10.3171/2015.6.JNS142203.

Chanraud, S., Zahr, N., Sullivan, E.V., and Pfefferbaum, A. (2010). MR diffusion tensor imaging: a window into white matter integrity of the working brain. *Neuropsychol Rev* 20(2)**,** 209-225. doi: 10.1007/s11065-010-9129-7.

Cheung, J.S., Wang, E., Lo, E.H., and Sun, P.Z. (2012). Stratification of heterogeneous diffusion MRI ischemic lesion with kurtosis imaging: evaluation of mean diffusion and kurtosis MRI mismatch in an animal model of transient focal ischemia. *Stroke* 43(8)**,** 2252-2254. doi: 10.1161/STROKEAHA.112.661926.

Chiu, H.C., and Damasio, A.R. (1980). Human cerebral asymmetries evaluated by computed tomography. *J Neurol Neurosurg Psychiatry* 43(10)**,** 873-878. doi: 10.1136/jnnp.43.10.873.

Ciccarelli, O., Toosy, A.T., Parker, G.J., Wheeler-Kingshott, C.A., Barker, G.J., Miller, D.H., et al. (2003). Diffusion tractography based group mapping of major white-matter pathways in the human brain. *Neuroimage* 19(4)**,** 1545-1555. doi: 10.1016/s1053-8119(03)00190-3.

Clark, C.A., Barrick, T.R., Murphy, M.M., and Bell, B.A. (2003). White matter fiber

tracking in patients with space-occupying lesions of the brain: a new technique for neurosurgical planning? *Neuroimage* 20(3)**,** 1601-1608.

Delgado, A.F., Fahlstrom, M., Nilsson, M., Berntsson, S.G., Zetterling, M., Libard, S., et al. (2017). Diffusion Kurtosis Imaging of Gliomas Grades II and III - A Study of Perilesional Tumor Infiltration, Tumor Grades and Subtypes at Clinical Presentation. *Radiol Oncol* 51(2)**,** 121-129. doi: 10.1515/raon-2017-0010.

Delgado, A.F., Nilsson, M., Latini, F., Martensson, J., Zetterling, M., Berntsson, S.G., et al. (2016). Preoperative Quantitative MR Tractography Compared with Visual Tract Evaluation in Patients with Neuropathologically Confirmed Gliomas Grades II and III: A Prospective Cohort Study. *Radiol Res Pract* 2016**,** 7671854. doi: 10.1155/2016/7671854.

Dhermain, F.G., Hau, P., Lanfermann, H., Jacobs, A.H., and van den Bent, M.J. (2010). Advanced MRI and PET imaging for assessment of treatment response in patients with gliomas. *Lancet Neurol* 9(9)**,** 906-920. doi: 10.1016/S1474-4422(10)70181-2.

Di Paola, M., Spalletta, G., and Caltagirone, C. (2010). In vivo structural neuroanatomy of corpus callosum in Alzheimer's disease and mild cognitive impairment using different MRI techniques: a review. *J Alzheimers Dis* 20(1)**,** 67-95. doi: 10.3233/JAD-2010-1370.

Dick, A.S., and Tremblay, P. (2012). Beyond the arcuate fasciculus: consensus and controversy in the connectional anatomy of language. *Brain* 135(Pt 12)**,** 3529-3550. doi: 10.1093/brain/aws222.

Dirven, L., Aaronson, N.K., Heimans, J.J., and Taphoorn, M.J. (2014). Health-related quality of life in high-grade glioma patients. *Chin J Cancer* 33(1)**,** 40-45. doi: 10.5732/cjc.013.10214.

Dong, X., Noorbakhsh, A., Hirshman, B.R., Zhou, T., Tang, J.A., Chang, D.C., et al. (2016). Survival trends of grade I, II, and III astrocytoma patients and associated clinical practice patterns between 1999 and 2010: A SEER-based analysis. *Neurooncol Pract* 3(1)**,** 29-38. doi: 10.1093/nop/npv016.

Douek, P., Turner, R., Pekar, J., Patronas, N., and Le Bihan, D. (1991). MR color mapping of myelin fiber orientation. *J Comput Assist Tomogr* 15(6)**,** 923-929. doi: 10.1097/00004728-199111000-00003.

Dubey, A., Kataria, R., and Sinha, V.D. (2018). Role of Diffusion Tensor Imaging in Brain Tumor Surgery. *Asian J Neurosurg* 13(2)**,** 302-306. doi: 10.4103/ajns.AJNS_226_16.

Falangola, M.F., Jensen, J.H., Babb, J.S., Hu, C., Castellanos, F.X., Di Martino, A., et al. (2008). Age-related non-Gaussian diffusion patterns in the prefrontal brain. *J Magn Reson Imaging* 28(6)**,** 1345-1350. doi: 10.1002/jmri.21604.

Falangola, M.F., Jensen, J.H., Tabesh, A., Hu, C., Deardorff, R.L., Babb, J.S., et al. (2013). Non-Gaussian diffusion MRI assessment of brain microstructure in mild cognitive impairment and Alzheimer's disease. *Magn Reson Imaging* 31(6)**,** 840-846. doi: 10.1016/j.mri.2013.02.008.

Falk Delgado, A., Nilsson, M., van Westen, D., and Falk Delgado, A. (2018). Glioma Grade Discrimination with MR Diffusion Kurtosis Imaging: A Meta-Analysis of Diagnostic Accuracy. *Radiology* 287(1)**,** 119-127. doi: 10.1148/radiol.2017171315.

Farshidfar, Z., Faeghi, F., Mohseni, M., Seddighi, A., Kharrazi, H.H., and Abdolmohammadi, J. (2014). Diffusion tensor tractography in the presurgical assessment of cerebral gliomas. *Neuroradiol J* 27(1)**,** 75-84. doi: 10.15274/NRJ-2014-10008.

Feng, W., Wang, J., Chhatbar, P.Y., Doughty, C., Landsittel, D., Lioutas, V.A., et al. (2015). Corticospinal tract lesion load: An imaging biomarker for stroke motor outcomes. *Ann Neurol* 78(6)**,** 860-870. doi: 10.1002/ana.24510.

Field, A.S., Alexander, A.L., Wu, Y.C., Hasan, K.M., Witwer, B., and Badie, B. (2004). Diffusion tensor eigenvector directional color imaging patterns in the evaluation of cerebral white matter tracts altered by tumor. *J Magn Reson Imaging* 20(4)**,** 555-562. doi: 10.1002/jmri.20169.

Foundas, A.L., Eure, K.F., Luevano, L.F., and Weinberger, D.R. (1998). MRI asymmetries of Broca's area: the pars triangularis and pars opercularis. *Brain Lang*

64(3), 282-296. doi: 10.1006/brln.1998.1974.

Gao, B., Shen, X., Shiroishi, M.S., Pang, M., Li, Z., Yu, B., et al. (2017). A pilot study of pre-operative motor dysfunction from gliomas in the region of corticospinal tract: Evaluation with diffusion tensor imaging. *PLoS One* 12(8), e0182795. doi: 10.1371/journal.pone.0182795.

Glasser, M.F., and Rilling, J.K. (2008). DTI tractography of the human brain's language pathways. *Cereb Cortex* 18(11), 2471-2482. doi: 10.1093/cercor/bhn011.

Gomez-Gastiasoro, A., Zubiaurre-Elorza, L., Pena, J., Ibarretxe-Bilbao, N., Rilo, O., Schretlen, D.J., et al. (2019). Altered frontal white matter asymmetry and its implications for cognition in schizophrenia: A tractography study. *Neuroimage Clin* 22, 101781. doi: 10.1016/j.nicl.2019.101781.

Gong, G., Jiang, T., Zhu, C., Zang, Y., He, Y., Xie, S., et al. (2005a). Side and handedness effects on the cingulum from diffusion tensor imaging. *Neuroreport* 16(15), 1701-1705.

Gong, G., Jiang, T., Zhu, C., Zang, Y., Wang, F., Xie, S., et al. (2005b). Asymmetry analysis of cingulum based on scale-invariant parameterization by diffusion tensor imaging. *Hum Brain Mapp* 24(2), 92-98. doi: 10.1002/hbm.20072.

Good, C.D., Johnsrude, I., Ashburner, J., Henson, R.N., Friston, K.J., and Frackowiak, R.S. (2001). Cerebral asymmetry and the effects of sex and handedness on brain structure: a voxel-based morphometric analysis of 465 normal adult human brains. *Neuroimage* 14(3), 685-700. doi: 10.1006/nimg.2001.0857.

Guan, J., Ma, X., Geng, Y., Qi, D., Shen, Y., Shen, Z., et al. (2019). Diffusion Kurtosis Imaging for Detection of Early Brain Changes in Parkinson's Disease. *Front Neurol* 10, 1285. doi: 10.3389/fneur.2019.01285.

Hasan, K.M., Iftikhar, A., Kamali, A., Kramer, L.A., Ashtari, M., Cirino, P.T., et al. (2009). Development and aging of the healthy human brain uncinate fasciculus across the lifespan using diffusion tensor tractography. *Brain Res* 1276, 67-76. doi: 10.1016/j.brainres.2009.04.025.

Hasan, K.M., Kamali, A., Abid, H., Kramer, L.A., Fletcher, J.M., and Ewing-Cobbs, L. (2010). Quantification of the spatiotemporal microstructural organization of the human brain association, projection and commissural pathways across the lifespan using diffusion tensor tractography. *Brain Struct Funct* 214(4)**,** 361-373. doi: 10.1007/s00429-009-0238-0.

Ho, M.L., Rojas, R., and Eisenberg, R.L. (2012). Cerebral edema. *AJR Am J Roentgenol* 199(3)**,** W258-273. doi: 10.2214/AJR.11.8081.

Hoeft, F., Barnea-Goraly, N., Haas, B.W., Golarai, G., Ng, D., Mills, D., et al. (2007). More is not always better: increased fractional anisotropy of superior longitudinal fasciculus associated with poor visuospatial abilities in Williams syndrome. *J Neurosci* 27(44)**,** 11960-11965. doi: 10.1523/JNEUROSCI.3591-07.2007.

Holly, K.S., Barker, B.J., Murcia, D., Bennett, R., Kalakoti, P., Ledbetter, C., et al. (2017). High-grade Gliomas Exhibit Higher Peritumoral Fractional Anisotropy and Lower Mean Diffusivity than Intracranial Metastases. *Front Surg* 4**,** 18. doi: 10.3389/fsurg.2017.00018.

Hua, K., Zhang, J., Wakana, S., Jiang, H., Li, X., Reich, D.S., et al. (2008). Tract probability maps in stereotaxic spaces: analyses of white matter anatomy and tract-specific quantification. *Neuroimage* 39(1)**,** 336-347. doi: 10.1016/j.neuroimage.2007.07.053.

Hui, E.S., Du, F., Huang, S., Shen, Q., and Duong, T.Q. (2012). Spatiotemporal dynamics of diffusional kurtosis, mean diffusivity and perfusion changes in experimental stroke. *Brain Res* 1451**,** 100-109. doi: 10.1016/j.brainres.2012.02.044.

Huster, R.J., Westerhausen, R., Kreuder, F., Schweiger, E., and Wittling, W. (2009). Hemispheric and gender related differences in the midcingulum bundle: a DTI study. *Hum Brain Mapp* 30(2)**,** 383-391. doi: 10.1002/hbm.20509.

Imfeld, A., Oechslin, M.S., Meyer, M., Loenneker, T., and Jancke, L. (2009). White matter plasticity in the corticospinal tract of musicians: a diffusion tensor imaging study. *Neuroimage* 46(3)**,** 600-607. doi: 10.1016/j.neuroimage.2009.02.025.

Inglese, M., and Bester, M. (2010). Diffusion imaging in multiple sclerosis: research and clinical implications. *NMR Biomed* 23(7)**,** 865-872. doi: 10.1002/nbm.1515.

Inoue, T., Ogasawara, K., Beppu, T., Ogawa, A., and Kabasawa, H. (2005). Diffusion tensor imaging for preoperative evaluation of tumor grade in gliomas. *Clin Neurol Neurosurg* 107(3)**,** 174-180. doi: 10.1016/j.clineuro.2004.06.011.

Jahanshad, N., Lee, A.D., Barysheva, M., McMahon, K.L., de Zubicaray, G.I., Martin, N.G., et al. (2010). Genetic influences on brain asymmetry: a DTI study of 374 twins and siblings. *Neuroimage* 52(2)**,** 455-469. doi: 10.1016/j.neuroimage.2010.04.236.

Jensen, J.H., and Helpern, J.A. (2010). MRI quantification of non-Gaussian water diffusion by kurtosis analysis. *NMR Biomed* 23(7)**,** 698-710. doi: 10.1002/nbm.1518.

Jensen, J.H., Helpern, J.A., Ramani, A., Lu, H., and Kaczynski, K. (2005a). Diffusional kurtosis imaging: the quantification of non-gaussian water diffusion by means of magnetic resonance imaging. *Magn Reson Med* 53(6)**,** 1432-1440. doi: 10.1002/mrm.20508.

Jensen, J.H., Helpern, J.A., Ramani, A., Lu, H.Z., and Kaczynski, K. (2005b). Diffusional kurtosis imaging: The quantification of non-Gaussian water diffusion by means of magnetic resonance imaging. *Magnetic Resonance in Medicine* 53(6)**,** 1432-1440. doi: 10.1002/mrm.20508.

Jiang, L., Xiao, C.Y., Xu, Q., Sun, J., Chen, H., Chen, Y.C., et al. (2017). Analysis of DTI-Derived Tensor Metrics in Differential Diagnosis between Low-grade and High-grade Gliomas. *Front Aging Neurosci* 9**,** 271. doi: 10.3389/fnagi.2017.00271.

Jiang, R., Jiang, J., Zhao, L., Zhang, J., Zhang, S., Yao, Y., et al. (2015). Diffusion kurtosis imaging can efficiently assess the glioma grade and cellular proliferation. *Oncotarget* 6(39)**,** 42380-42393. doi: 10.18632/oncotarget.5675.

Jones, D.K., Christiansen, K.F., Chapman, R.J., and Aggleton, J.P. (2013). Distinct subdivisions of the cingulum bundle revealed by diffusion MRI fibre tracking: implications for neuropsychological investigations. *Neuropsychologia* 51(1)**,** 67-78. doi: 10.1016/j.neuropsychologia.2012.11.018.

Kansaku, K., Yamaura, A., and Kitazawa, S. (2000). Sex differences in lateralization revealed in the posterior language areas. *Cereb Cortex* 10(9)**,** 866-872. doi: 10.1093/cercor/10.9.866.

Karger, J. (1985). Nmr Self-Diffusion Studies in Heterogeneous Systems. *Advances in Colloid and Interface Science* 23(1-4)**,** 129-148. doi: Doi 10.1016/0001-8686(85)80018-X.

Keles, G.E., Chang, E.F., Lamborn, K.R., Tihan, T., Chang, C.J., Chang, S.M., et al. (2006). Volumetric extent of resection and residual contrast enhancement on initial surgery as predictors of outcome in adult patients with hemispheric anaplastic astrocytoma. *J Neurosurg* 105(1)**,** 34-40. doi: 10.3171/jns.2006.105.1.34.

Kikinis, R., and Pieper, S. (2011). 3D Slicer as a tool for interactive brain tumor segmentation. *Conf Proc IEEE Eng Med Biol Soc* 2011**,** 6982-6984. doi: 10.1109/IEMBS.2011.6091765.

Kleihues, P., Soylemezoglu, F., Schauble, B., Scheithauer, B.W., and Burger, P.C. (1995). Histopathology, classification, and grading of gliomas. *Glia* 15(3)**,** 211-221. doi: 10.1002/glia.440150303.

Koay, C.G., Chang, L.C., Carew, J.D., Pierpaoli, C., and Basser, P.J. (2006). A unifying theoretical and algorithmic framework for least squares methods of estimation in diffusion tensor imaging. *J Magn Reson* 182(1)**,** 115-125. doi: 10.1016/j.jmr.2006.06.020.

Kubicki, M., McCarley, R., Westin, C.F., Park, H.J., Maier, S., Kikinis, R., et al. (2007). A review of diffusion tensor imaging studies in schizophrenia. *J Psychiatr Res* 41(1-2)**,** 15-30. doi: 10.1016/j.jpsychires.2005.05.005.

Kubicki, M., Westin, C.F., Maier, S.E., Frumin, M., Nestor, P.G., Salisbury, D.F., et al. (2002). Uncinate fasciculus findings in schizophrenia: a magnetic resonance diffusion tensor imaging study. *Am J Psychiatry* 159(5)**,** 813-820. doi: 10.1176/appi.ajp.159.5.813.

Kuhnt, D., Becker, A., Ganslandt, O., Bauer, M., Buchfelder, M., and Nimsky, C. (2011).

Correlation of the extent of tumor volume resection and patient survival in surgery of glioblastoma multiforme with high-field intraoperative MRI guidance. *Neuro Oncol* 13(12)**,** 1339-1348. doi: 10.1093/neuonc/nor133.

Lanzafame, S., Giannelli, M., Garaci, F., Floris, R., Duggento, A., Guerrisi, M., et al. (2016). Differences in Gaussian diffusion tensor imaging and non-Gaussian diffusion kurtosis imaging model-based estimates of diffusion tensor invariants in the human brain. *Med Phys* 43(5)**,** 2464. doi: 10.1118/1.4946819.

Latt, J., Nilsson, M., Wirestam, R., Stahlberg, F., Karlsson, N., Johansson, M., et al. (2013). Regional values of diffusional kurtosis estimates in the healthy brain. *J Magn Reson Imaging* 37(3)**,** 610-618. doi: 10.1002/jmri.23857.

Lazar, M., Jensen, J.H., Xuan, L., and Helpern, J.A. (2008). Estimation of the orientation distribution function from diffusional kurtosis imaging. *Magn Reson Med* 60(4)**,** 774-781. doi: 10.1002/mrm.21725.

Le Bihan, D., Breton, E., Lallemand, D., Aubin, M.L., Vignaud, J., and Laval-Jeantet, M. (1988). Separation of diffusion and perfusion in intravoxel incoherent motion MR imaging. *Radiology* 168(2)**,** 497-505. doi: 10.1148/radiology.168.2.3393671.

Le Bihan, D., Breton, E., Lallemand, D., Grenier, P., Cabanis, E., and Laval-Jeantet, M. (1986). MR imaging of intravoxel incoherent motions: application to diffusion and perfusion in neurologic disorders. *Radiology* 161(2)**,** 401-407. doi: 10.1148/radiology.161.2.3763909.

Le Bihan, D., Mangin, J.F., Poupon, C., Clark, C.A., Pappata, S., Molko, N., et al. (2001). Diffusion tensor imaging: concepts and applications. *J Magn Reson Imaging* 13(4)**,** 534-546. doi: 10.1002/jmri.1076.

Lebel, C., and Beaulieu, C. (2009). Lateralization of the arcuate fasciculus from childhood to adulthood and its relation to cognitive abilities in children. *Hum Brain Mapp* 30(11)**,** 3563-3573. doi: 10.1002/hbm.20779.

Lee, C.Y., Tabesh, A., Nesland, T., Jensen, J.H., Helpern, J.A., Spampinato, M.V., et al. (2014). Human brain asymmetry in microstructural connectivity demonstrated by

diffusional kurtosis imaging. *Brain Res* 1588**,** 73-80. doi: 10.1016/j.brainres.2014.09.002.

LeMay, M. (1977). Asymmetries of the skull and handedness. Phrenology revisited. *J Neurol Sci* 32(2)**,** 243-253. doi: 10.1016/0022-510x(77)90239-8.

Li, L., Preuss, T.M., Rilling, J.K., Hopkins, W.D., Glasser, M.F., Kumar, B., et al. (2010). Chimpanzee (Pan troglodytes) precentral corticospinal system asymmetry and handedness: a diffusion magnetic resonance imaging study. *PLoS One* 5(9)**,** e12886. doi: 10.1371/journal.pone.0012886.

Lu, S., Ahn, D., Johnson, G., and Cha, S. (2003). Peritumoral diffusion tensor imaging of high-grade gliomas and metastatic brain tumors. *AJNR Am J Neuroradiol* 24(5)**,** 937-941.

Luders, E., Gaser, C., Jancke, L., and Schlaug, G. (2004). A voxel-based approach to gray matter asymmetries. *Neuroimage* 22(2)**,** 656-664. doi: 10.1016/j.neuroimage.2004.01.032.

Lurito, J.T., and Dzemidzic, M. (2001). Determination of cerebral hemisphere language dominance with functional magnetic resonance imaging. *Neuroimaging Clin N Am* 11(2)**,** 355-363, x.

Makris, N., Kennedy, D.N., McInerney, S., Sorensen, A.G., Wang, R., Caviness, V.S., Jr., et al. (2005). Segmentation of subcomponents within the superior longitudinal fascicle in humans: a quantitative, in vivo, DT-MRI study. *Cereb Cortex* 15(6)**,** 854-869. doi: 10.1093/cercor/bhh186.

Mamah, D., Conturo, T.E., Harms, M.P., Akbudak, E., Wang, L., McMichael, A.R., et al. (2010). Anterior thalamic radiation integrity in schizophrenia: a diffusion-tensor imaging study. *Psychiatry Res* 183(2)**,** 144-150. doi: 10.1016/j.pscychresns.2010.04.013.

Mandonnet, E., Nouet, A., Gatignol, P., Capelle, L., and Duffau, H. (2007). Does the left inferior longitudinal fasciculus play a role in language? A brain stimulation study. *Brain* 130(Pt 3)**,** 623-629. doi: 10.1093/brain/awl361.

Marchina, S., Zhu, L.L., Norton, A., Zipse, L., Wan, C.Y., and Schlaug, G. (2011). Impairment of speech production predicted by lesion load of the left arcuate fasciculus. *Stroke* 42(8)**,** 2251-2256. doi: 10.1161/STROKEAHA.110.606103.

Morita, N., Wang, S., Kadakia, P., Chawla, S., Poptani, H., and Melhem, E.R. (2011). Diffusion tensor imaging of the corticospinal tract in patients with brain neoplasms. *Magn Reson Med Sci* 10(4)**,** 239-243. doi: 10.2463/mrms.10.239.

Nichols, T.E., and Holmes, A.P. (2002). Nonparametric permutation tests for functional neuroimaging: a primer with examples. *Hum Brain Mapp* 15(1)**,** 1-25. doi: 10.1002/hbm.1058.

Nimsky, C. (2011). Intraoperative acquisition of fMRI and DTI. *Neurosurg Clin N Am* 22(2)**,** 269-277, ix. doi: 10.1016/j.nec.2010.11.005.

O'Donnell, L.J., Westin, C.F., and Golby, A.J. (2009). Tract-based morphometry for white matter group analysis. *Neuroimage* 45(3)**,** 832-844. doi: 10.1016/j.neuroimage.2008.12.023.

Ojemann, J.G., Miller, J.W., and Silbergeld, D.L. (1996). Preserved function in brain invaded by tumor. *Neurosurgery* 39(2)**,** 253-258; discussion 258-259. doi: 10.1097/00006123-199608000-00003.

Park, H.J., Westin, C.F., Kubicki, M., Maier, S.E., Niznikiewicz, M., Baer, A., et al. (2004). White matter hemisphere asymmetries in healthy subjects and in schizophrenia: a diffusion tensor MRI study. *Neuroimage* 23(1)**,** 213-223. doi: 10.1016/j.neuroimage.2004.04.036.

Pope, W.B., and Brandal, G. (2018). Conventional and advanced magnetic resonance imaging in patients with high-grade glioma. *Q J Nucl Med Mol Imaging* 62(3)**,** 239-253. doi: 10.23736/S1824-4785.18.03086-8.

Powell, H.W., Parker, G.J., Alexander, D.C., Symms, M.R., Boulby, P.A., Wheeler-Kingshott, C.A., et al. (2006). Hemispheric asymmetries in language-related pathways: a combined functional MRI and tractography study. *Neuroimage* 32(1)**,** 388-399. doi: 10.1016/j.neuroimage.2006.03.011.

Price, S.J., Pena, A., Burnet, N.G., Jena, R., Green, H.A., Carpenter, T.A., et al. (2004). Tissue signature characterisation of diffusion tensor abnormalities in cerebral gliomas. *Eur Radiol* 14(10)**,** 1909-1917. doi: 10.1007/s00330-004-2381-6.

Puig, J., Pedraza, S., Blasco, G., Daunis, I.E.J., Prados, F., Remollo, S., et al. (2011). Acute damage to the posterior limb of the internal capsule on diffusion tensor tractography as an early imaging predictor of motor outcome after stroke. *AJNR Am J Neuroradiol* 32(5)**,** 857-863. doi: 10.3174/ajnr.A2400.

Pujol, J., Deus, J., Losilla, J.M., and Capdevila, A. (1999). Cerebral lateralization of language in normal left-handed people studied by functional MRI. *Neurology* 52(5)**,** 1038-1043. doi: 10.1212/wnl.52.5.1038.

Qi, C., Yang, S., Meng, L., Chen, H., Li, Z., Wang, S., et al. (2017). Evaluation of cerebral glioma using 3T diffusion kurtosis tensor imaging and the relationship between diffusion kurtosis metrics and tumor cellularity. *J Int Med Res* 45(4)**,** 1347-1358. doi: 10.1177/0300060517712654.

Qi, X.X., Shi, D.F., Ren, S.X., Zhang, S.Y., Li, L., Li, Q.C., et al. (2018). Histogram analysis of diffusion kurtosis imaging derived maps may distinguish between low and high grade gliomas before surgery. *Eur Radiol* 28(4)**,** 1748-1755. doi: 10.1007/s00330-017-5108-1.

Raab, P., Hattingen, E., Franz, K., Zanella, F.E., and Lanfermann, H. (2010). Cerebral gliomas: diffusional kurtosis imaging analysis of microstructural differences. *Radiology* 254(3)**,** 876-881. doi: 10.1148/radiol.09090819.

Rodrigo, S., Naggara, O., Oppenheim, C., Golestani, N., Poupon, C., Cointepas, Y., et al. (2007). Human subinsular asymmetry studied by diffusion tensor imaging and fiber tracking. *AJNR Am J Neuroradiol* 28(8)**,** 1526-1531. doi: 10.3174/ajnr.A0584.

Rosenstock, T., Giampiccolo, D., Schneider, H., Runge, S.J., Bahrend, I., Vajkoczy, P., et al. (2017). Specific DTI seeding and diffusivity-analysis improve the quality and prognostic value of TMS-based deterministic DTI of the pyramidal tract. *Neuroimage Clin* 16**,** 276-285. doi: 10.1016/j.nicl.2017.08.010.

Scherer, H.J. (1940). The forms of growth in gliomas and their practical significance. *Brain* 63**,** 1-35. doi: DOI 10.1093/brain/63.1.1.

Seizeur, R., Magro, E., Prima, S., Wiest-Daessle, N., Maumet, C., and Morandi, X. (2014). Corticospinal tract asymmetry and handedness in right- and left-handers by diffusion tensor tractography. *Surg Radiol Anat* 36(2)**,** 111-124. doi: 10.1007/s00276-013-1156-7.

Shapleske, J., Rossell, S.L., Woodruff, P.W., and David, A.S. (1999). The planum temporale: a systematic, quantitative review of its structural, functional and clinical significance. *Brain Res Brain Res Rev* 29(1)**,** 26-49. doi: 10.1016/s0165-0173(98)00047-2.

Shu, N., Liu, Y., Duan, Y., and Li, K. (2015). Hemispheric Asymmetry of Human Brain Anatomical Network Revealed by Diffusion Tensor Tractography. *Biomed Res Int* 2015**,** 908917. doi: 10.1155/2015/908917.

Silva, G., and Citterio, A. (2017). Hemispheric asymmetries in dorsal language pathway white-matter tracts: A magnetic resonance imaging tractography and functional magnetic resonance imaging study. *Neuroradiol J* 30(5)**,** 470-476. doi: 10.1177/1971400917720829.

Smith, S.M., Jenkinson, M., Johansen-Berg, H., Rueckert, D., Nichols, T.E., Mackay, C.E., et al. (2006). Tract-based spatial statistics: voxelwise analysis of multi-subject diffusion data. *Neuroimage* 31(4)**,** 1487-1505. doi: 10.1016/j.neuroimage.2006.02.024.

Smith, S.M., Jenkinson, M., Woolrich, M.W., Beckmann, C.F., Behrens, T.E., Johansen-Berg, H., et al. (2004). Advances in functional and structural MR image analysis and implementation as FSL. *Neuroimage* 23 Suppl 1**,** S208-219. doi: 10.1016/j.neuroimage.2004.07.051.

Soares, J.M., Marques, P., Alves, V., and Sousa, N. (2013). A hitchhiker's guide to diffusion tensor imaging. *Front Neurosci* 7**,** 31. doi: 10.3389/fnins.2013.00031.

Sreedharan, R.M., Menon, A.C., James, J.S., Kesavadas, C., and Thomas, S.V. (2015).

Arcuate fasciculus laterality by diffusion tensor imaging correlates with language laterality by functional MRI in preadolescent children. *Neuroradiology* 57(3)**,** 291-297. doi: 10.1007/s00234-014-1469-1.

Steinmetz, H. (1996). Structure, functional and cerebral asymmetry: in vivo morphometry of the planum temporale. *Neurosci Biobehav Rev* 20(4)**,** 587-591. doi: 10.1016/0149-7634(95)00071-2.

Steven, A.J., Zhuo, J., and Melhem, E.R. (2014). Diffusion kurtosis imaging: an emerging technique for evaluating the microstructural environment of the brain. *AJR Am J Roentgenol* 202(1)**,** W26-33. doi: 10.2214/AJR.13.11365.

Stupp, R., Hegi, M.E., Mason, W.P., van den Bent, M.J., Taphoorn, M.J., Janzer, R.C., et al. (2009). Effects of radiotherapy with concomitant and adjuvant temozolomide versus radiotherapy alone on survival in glioblastoma in a randomised phase III study: 5-year analysis of the EORTC-NCIC trial. *Lancet Oncol* 10(5)**,** 459-466. doi: 10.1016/S1470-2045(09)70025-7.

Sun, Z.Y., Kloppel, S., Riviere, D., Perrot, M., Frackowiak, R., Siebner, H., et al. (2012). The effect of handedness on the shape of the central sulcus. *Neuroimage* 60(1)**,** 332-339. doi: 10.1016/j.neuroimage.2011.12.050.

Sydnor, V.J., Rivas-Grajales, A.M., Lyall, A.E., Zhang, F., Bouix, S., Karmacharya, S., et al. (2018). A comparison of three fiber tract delineation methods and their impact on white matter analysis. *Neuroimage* 178**,** 318-331. doi: 10.1016/j.neuroimage.2018.05.044.

Szczepankiewicz, F., van Westen, D., Englund, E., Westin, C.F., Stahlberg, F., Latt, J., et al. (2016). The link between diffusion MRI and tumor heterogeneity: Mapping cell eccentricity and density by diffusional variance decomposition (DIVIDE). *Neuroimage* 142**,** 522-532. doi: 10.1016/j.neuroimage.2016.07.038.

Tabesh, A., Jensen, J.H., Ardekani, B.A., and Helpern, J.A. (2011). Estimation of tensors and tensor-derived measures in diffusional kurtosis imaging. *Magn Reson Med* 65(3)**,** 823-836. doi: 10.1002/mrm.22655.

Takao, H., Hayashi, N., and Ohtomo, K. (2011). White matter asymmetry in healthy individuals: a diffusion tensor imaging study using tract-based spatial statistics. *Neuroscience* 193**,** 291-299. doi: 10.1016/j.neuroscience.2011.07.041.

Tan, Y., Zhang, H., Zhao, R.F., Wang, X.C., Qin, J.B., and Wu, X.F. (2016). Comparison of the values of MRI diffusion kurtosis imaging and diffusion tensor imaging in cerebral astrocytoma grading and their association with aquaporin-4. *Neurol India* 64(2)**,** 265-272. doi: 10.4103/0028-3886.177621.

Thiebaut de Schotten, M., Ffytche, D.H., Bizzi, A., Dell'Acqua, F., Allin, M., Walshe, M., et al. (2011). Atlasing location, asymmetry and inter-subject variability of white matter tracts in the human brain with MR diffusion tractography. *Neuroimage* 54(1)**,** 49-59. doi: 10.1016/j.neuroimage.2010.07.055.

Thomalla, G., Glauche, V., Koch, M.A., Beaulieu, C., Weiller, C., and Rother, J. (2004). Diffusion tensor imaging detects early Wallerian degeneration of the pyramidal tract after ischemic stroke. *Neuroimage* 22(4)**,** 1767-1774. doi: 10.1016/j.neuroimage.2004.03.041.

Thomas, C., Humphreys, K., Jung, K.J., Minshew, N., and Behrmann, M. (2011). The anatomy of the callosal and visual-association pathways in high-functioning autism: a DTI tractography study. *Cortex* 47(7)**,** 863-873. doi: 10.1016/j.cortex.2010.07.006.

Toga, A.W., and Thompson, P.M. (2003). Mapping brain asymmetry. *Nat Rev Neurosci* 4(1)**,** 37-48. doi: 10.1038/nrn1009.

Tournier, J.D., Mori, S., and Leemans, A. (2011). Diffusion tensor imaging and beyond. *Magn Reson Med* 65(6)**,** 1532-1556. doi: 10.1002/mrm.22924.

Tuch, D.S., Reese, T.G., Wiegell, M.R., and Wedeen, V.J. (2003). Diffusion MRI of complex neural architecture. *Neuron* 40(5)**,** 885-895. doi: 10.1016/s0896-6273(03)00758-x.

Van Cauter, S., Veraart, J., Sijbers, J., Peeters, R.R., Himmelreich, U., De Keyzer, F., et al. (2012). Gliomas: diffusion kurtosis MR imaging in grading. *Radiology* 263(2)**,** 492-501. doi: 10.1148/radiol.12110927.

Veraart, J., Poot, D.H., Van Hecke, W., Blockx, I., Van der Linden, A., Verhoye, M., et al. (2011). More accurate estimation of diffusion tensor parameters using diffusion Kurtosis imaging. *Magn Reson Med* 65(1)**,** 138-145. doi: 10.1002/mrm.22603.

Veraart, J., Sijbers, J., Sunaert, S., Leemans, A., and Jeurissen, B. (2013). Weighted linear least squares estimation of diffusion MRI parameters: strengths, limitations, and pitfalls. *Neuroimage* 81**,** 335-346. doi: 10.1016/j.neuroimage.2013.05.028.

Virta, A., Barnett, A., and Pierpaoli, C. (1999). Visualizing and characterizing white matter fiber structure and architecture in the human pyramidal tract using diffusion tensor MRI. *Magn Reson Imaging* 17(8)**,** 1121-1133. doi: 10.1016/s0730-725x(99)00048-x.

Vogel, J.J., Bowers, C.A., and Vogel, D.S. (2003). Cerebral lateralization of spatial abilities: a meta-analysis. *Brain Cogn* 52(2)**,** 197-204. doi: 10.1016/s0278-2626(03)00056-3.

Wakana, S., Caprihan, A., Panzenboeck, M.M., Fallon, J.H., Perry, M., Gollub, R.L., et al. (2007). Reproducibility of quantitative tractography methods applied to cerebral white matter. *Neuroimage* 36(3)**,** 630-644. doi: 10.1016/j.neuroimage.2007.02.049.

Wakana, S., Jiang, H., Nagae-Poetscher, L.M., van Zijl, P.C., and Mori, S. (2004). Fiber tract-based atlas of human white matter anatomy. *Radiology* 230(1)**,** 77-87. doi: 10.1148/radiol.2301021640.

Wang, F., Sun, Z., Cui, L., Du, X., Wang, X., Zhang, H., et al. (2004). Anterior cingulum abnormalities in male patients with schizophrenia determined through diffusion tensor imaging. *Am J Psychiatry* 161(3)**,** 573-575. doi: 10.1176/appi.ajp.161.3.573.

Wang, J.J., Lin, W.Y., Lu, C.S., Weng, Y.H., Ng, S.H., Wang, C.H., et al. (2011). Parkinson disease: diagnostic utility of diffusion kurtosis imaging. *Radiology* 261(1)**,** 210-217. doi: 10.1148/radiol.11102277.

Wang, X., Gao, W., Li, F., Shi, W., Li, H., and Zeng, Q. (2019). Diffusion kurtosis imaging as an imaging biomarker for predicting prognosis of the patients with high-grade gliomas. *Magn Reson Imaging* 63**,** 131-136. doi: 10.1016/j.mri.2019.08.001.

Ward, N.S., Newton, J.M., Swayne, O.B., Lee, L., Thompson, A.J., Greenwood, R.J., et al. (2006). Motor system activation after subcortical stroke depends on corticospinal system integrity. *Brain* 129(Pt 3)**,** 809-819. doi: 10.1093/brain/awl002.

Westerhausen, R., Huster, R.J., Kreuder, F., Wittling, W., and Schweiger, E. (2007). Corticospinal tract asymmetries at the level of the internal capsule: is there an association with handedness? *Neuroimage* 37(2)**,** 379-386. doi: 10.1016/j.neuroimage.2007.05.047.

Wilde, E.A., McCauley, S.R., Chu, Z., Hunter, J.V., Bigler, E.D., Yallampalli, R., et al. (2009). Diffusion tensor imaging of hemispheric asymmetries in the developing brain. *J Clin Exp Neuropsychol* 31(2)**,** 205-218. doi: 10.1080/13803390802098118.

Winkler, A.M., Ridgway, G.R., Webster, M.A., Smith, S.M., and Nichols, T.E. (2014). Permutation inference for the general linear model. *Neuroimage* 92**,** 381-397. doi: 10.1016/j.neuroimage.2014.01.060.

Woolrich, M.W., Jbabdi, S., Patenaude, B., Chappell, M., Makni, S., Behrens, T., et al. (2009). Bayesian analysis of neuroimaging data in FSL. *Neuroimage* 45(1 Suppl)**,** S173-186. doi: 10.1016/j.neuroimage.2008.10.055.

Yablonskiy, D.A., Bretthorst, G.L., and Ackerman, J.J. (2003). Statistical model for diffusion attenuated MR signal. *Magn Reson Med* 50(4)**,** 664-669. doi: 10.1002/mrm.10578.

Yamada, K., Kizu, O., Mori, S., Ito, H., Nakamura, H., Yuen, S., et al. (2003). Brain fiber tracking with clinically feasible diffusion-tensor MR imaging: initial experience. *Radiology* 227(1)**,** 295-301. doi: 10.1148/radiol.2271020313.

Yasmin, H., Aoki, S., Abe, O., Nakata, Y., Hayashi, N., Masutani, Y., et al. (2009). Tract-specific analysis of white matter pathways in healthy subjects: a pilot study using diffusion tensor MRI. *Neuroradiology* 51(12)**,** 831-840. doi: 10.1007/s00234-009-0580-1.

Yeatman, J.D., Dougherty, R.F., Myall, N.J., Wandell, B.A., and Feldman, H.M. (2012). Tract profiles of white matter properties: automating fiber-tract quantification. *PLoS*

One 7(11)**,** e49790. doi: 10.1371/journal.pone.0049790.

Yeh, F.C., and Tseng, W.Y. (2011). NTU-90: a high angular resolution brain atlas constructed by q-space diffeomorphic reconstruction. *Neuroimage* 58(1)**,** 91-99. doi: 10.1016/j.neuroimage.2011.06.021.

Yendiki, A., Panneck, P., Srinivasan, P., Stevens, A., Zollei, L., Augustinack, J., et al. (2011). Automated probabilistic reconstruction of white-matter pathways in health and disease using an atlas of the underlying anatomy. *Front Neuroinform* 5**,** 23. doi: 10.3389/fninf.2011.00023.

Yong, R.L., and Lonser, R.R. (2011). Surgery for glioblastoma multiforme: striking a balance. *World Neurosurg* 76(6)**,** 528-530. doi: 10.1016/j.wneu.2011.06.053.

Yu, V.Y., MacDonald, M.J., Oh, A., Hua, G.N., De Nil, L.F., and Pang, E.W. (2014). Age-related sex differences in language lateralization: A magnetoencephalography study in children. *Dev Psychol* 50(9)**,** 2276-2284. doi: 10.1037/a0037470.

Zhou, X.X., Li, X.H., Chen, D.B., Wu, C., Feng, L., Chu, J.P., et al. (2018). The asymmetry of neural symptoms in Wilson's disease patients detecting by diffusion tensor imaging, resting-state functional MRI, and susceptibility-weighted imaging. *Brain Behav* 8(5)**,** e00930. doi: 10.1002/brb3.930.

Zhu, J., Zhuo, C., Qin, W., Wang, D., Ma, X., Zhou, Y., et al. (2015). Performances of diffusion kurtosis imaging and diffusion tensor imaging in detecting white matter abnormality in schizophrenia. *Neuroimage Clin* 7**,** 170-176. doi: 10.1016/j.nicl.2014.12.008.

Zhu, L.L., Lindenberg, R., Alexander, M.P., and Schlaug, G. (2010). Lesion load of the corticospinal tract predicts motor impairment in chronic stroke. *Stroke* 41(5)**,** 910-915. doi: 10.1161/STROKEAHA.109.577023.

Zhuo, J., Keledjian, K., Xu, S., Pampori, A., Gerzanich, V., Simard, J.M., et al. (2015). Changes in Diffusion Kurtosis Imaging and Magnetic Resonance Spectroscopy in a Direct Cranial Blast Traumatic Brain Injury (dc-bTBI) Model. *PLoS One* 10(8)**,** e0136151. doi: 10.1371/journal.pone.0136151.

List of Academic Teachers

My academic teachers in Marburg were:

Prof. Dr. Christopher Nimsky, Dr. Miriam Bopp

Astrid Burmester, Katrin Diewock, Michaela Dürwald, Sabine Ferber, Akkiko Sawatari-Elter

Note of Thanks

At the end of the dissertation, I want to express my thanks to those who supported me during my study in Marburg.

I would like to thank Prof. Dr. Ch. Nimsky for kindly offering me the chance to study in Marburg and join in the morning conference and learn by observation in the OR. Those cases inspired me to research the topics of my dissertation.

Also, I want to thank Dr. M. Bopp, who always tried her best to help me whenever I came across problems in my research. She sparked my interest in the field of multi-modal imaging analysis and introduced a great deal of software to me that would be of great help.

Furthermore, I want to thank Prof. Dr. J. W. Bartsch for helping me revise the language of my dissertation and who was always ready to help and to share knowledge.

Moreover, I want to thank my best friend Lixian Liu, who always listens and talks to me when I'm upset.

Last but not the least, I want to thank my parents for their mental support even if they are not by my side. Without them, I could not have endured all the loneliness and pain during my stay in a foreign country, neither could I have finished writing my dissertation.